Chapter 4
Blast Cleaning Equipment

4.1 General Structure of Blast Cleaning Systems

The general structure of a pressure blast cleaning system is illustrated in Fig. 4.1. It basically consists of two types of equipment: air suppliers and air consumers. The prime *air supplier* is the compressor. At larger sites, storage pressure vessels accompany a compressor. These vessels serve to store a certain amount of pressurised air, and to allow an unrestricted delivery of a demanded amount of compressed air to the consumers. The prime *air consumer* is the blast cleaning nozzle. However, hoses, whether air hoses or abrasive hoses, are air consumers as well – a fact which is often not considered. Another consumer is the breathing air system. However, it is not uncommon to run separate small compressors for breathing air supply; an example is shown in Fig. 4.1. Further parts of a blast cleaning configuration are control devices, valve arrangements and safety equipment.

4.2 Air Compressors

4.2.1 General Aspects

Compressed air can be generated by several methods as illustrated in Fig. 4.2. For industrial applications, the most frequently type used is the screw compressor. Screw compressors are available in two variants: oil-lubricated and oil-free. Table 4.1 lists technical data of screw compressors routinely used for on-site blast cleaning operations. Screw compressors feature the following advantages:

- no wear because of the frictionless movements of male and female rotors;
- adjustable internal compression;
- high rotational speeds (up to 15,000/min);
- small dimensions.

The fundamental principle for screw compaction was already invented and patented in 1878. It is based on the opposite rotation of two helical rotors with aligned profiles. The two rotors are named as male and female rotors, respectively.

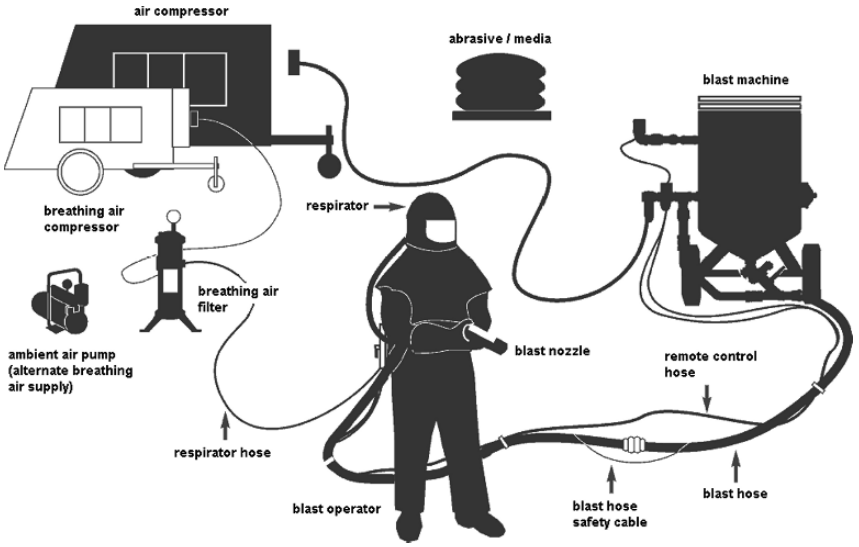

Fig. 4.1 Basic parts of a compressed air system for blast cleaning operations (Clemco Inc., Washington)

The air to be compacted will be sucked into the compressor via an air filter. The air will be compacted in the closed room generated between cylinder wall and the teeth of the two rotors. The sealing between screws and body is due to oil injection. This oil, that also lubricates the bearings and absorbs part of the process heat, will later be removed with the aid of an oil separator. Therefore, oiled screw compressors cause rather low maintenance costs.

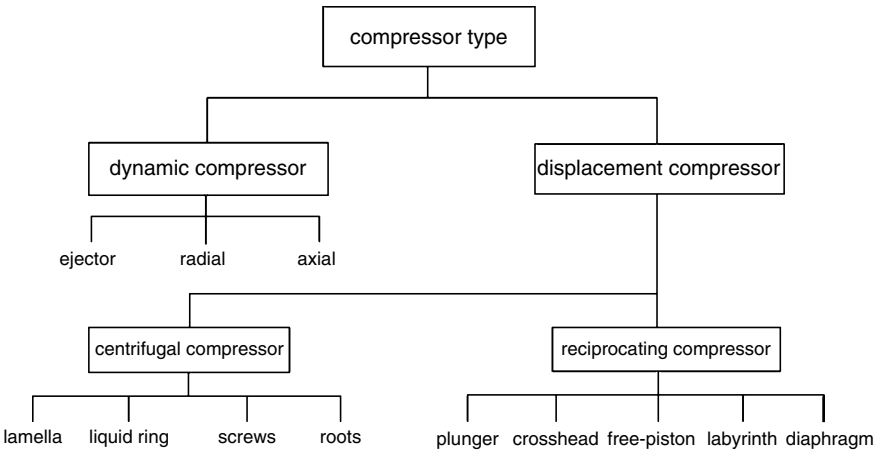

Fig. 4.2 Compressor types for air compression (Ruppelt, 2003)

Table 4.1 Technical data of mobile screw compressors (Atlas Copco GmbH, Essen)

Type	Unit	XAHS 365	XAHS 350	XAS 125
Nominal pressure	MPa	1.2	1.2	0.7
Nominal volumetric flow rate	m^3/min	21.5	20.4	7.5
Power rating in kW	kW	206		
Length total	mm	4,210	4,650	4,177
Width total	mm	1,810	1,840	1,660
Height total	mm	2,369	2,250	1,527
Weight (empty)	kg	3,800		
Weight (ready for operation)	kg	4,300	4,500	1,430
Air exit valves	–	$1 \times 2'' + 1 \times 1''$	$1 \times 1/4'' + 1 \times 3/4''$	$1/4'' + 3 \times 3/4''$
Noise level	dB (A)	74	75	71

The displaced volume per revolution of the male rotor not only depends on diameter and length of the rotor but also on its profile. One revolution of the main helical rotor conveys a unit volume q_0, and the theoretical flow rate for the compressor reads as follows:

$$\dot{Q}_0 = n_C \cdot q_0 \tag{4.1}$$

The actual flow rate, however, is lowered by lost volume; the amount of which depends on the total cross-section of clearances, air density, compression ratio, peripheral speed of rotor and built-in volume ratio. More information is available in standard textbooks (Bendler, 1983; Bloch, 1995; Groth, 1995).

4.2.2 Working Lines

A working line of a compressor is defined as follows:

$$p = f(\dot{Q}_A) \tag{4.2}$$

where p is the pressure delivered by the compressor and $\dot{Q}_A$ is the volumetric air flow rate. The precise shape of (4.2) depends on the compressor type. A working line of a screw compressor is shown in Fig. 4.3 together with the working lines for three nozzles with different nozzle diameters. The working lines for nozzles can be established according to the procedure outlined in Sect. 3.2.1.

It can be seen in Fig. 4.3 that the working line of the compressors and the working lines of two nozzles intersect. The intersection points are called *working points* of the system. This point characterises the parameter combination for the most effective performance of the system. If a compressor type is given, the positions of the individual working points depend on the nozzle to be used. These points are designated "II" for the nozzle "2" with $d_N = 10$ mm and "III" for the nozzle "3" with $d_N = 12$ mm. The horizontal dotted line in Fig. 4.3 characterises the pressure limit for the compressor; and it is at $p = 1.3$ MPa. It can be seen that

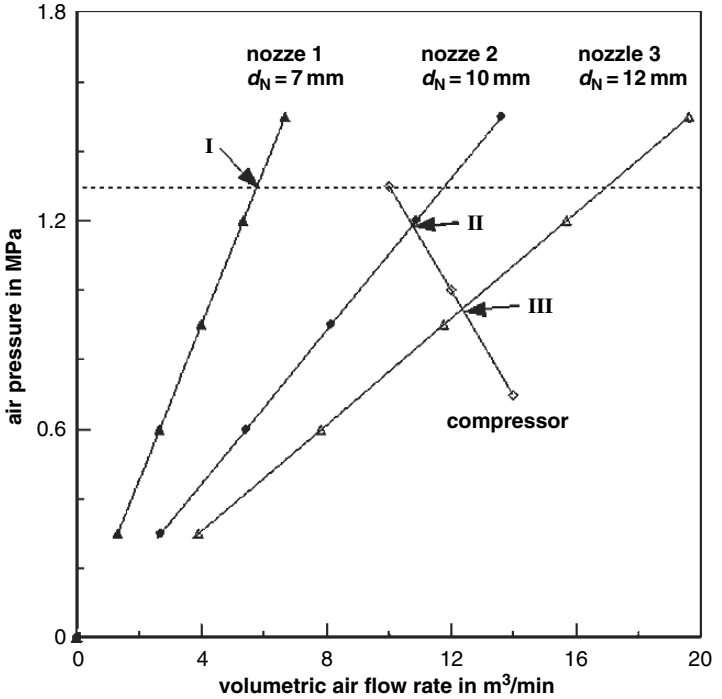

Fig. 4.3 Working lines of a screw compressor and of three blast cleaning nozzles

the working line of the nozzle "1" with $d_N = 7$ mm does not cross the working line of the compressor, but it intersects with the dotted line (point "I"). Because the cross-section of this nozzle is rather small, it requires a high pressure for the transport of a given air volumetric flow rate through the cross-section. This high pressure cannot be provided by the compressor. The dotted line also expresses the volumetric air flow rate capabilities for the other two nozzles. These values can be estimated from the points where working line and dotted line intersect. The critical volumetric flow rate is $\dot{Q}_A = 12\,m^3/min$ for nozzle "2", and it is $\dot{Q}_A = 17\,m^3/min$ for nozzle "3". The compressor cannot deliver these high values; its capacity is limited to $\dot{Q}_A = 10\,m^3/min$ for $p = 1.3$ MPa, which can be read from the working line of the compressor. However, the calculations help to design a buffer vessel, which can deliver the required volumetric air flow rates.

4.2.3 Power Rating

If isentropic compression is assumed (entropy remains constant during the compression), the theoretical power required to lift a given air volume flow rate from a

pressure level p_1 up to a pressure level p_2 can be derived from the work done on isentropic compression. This power can be calculated as follows (Bendler, 1983):

$$P_H = \frac{\kappa}{\kappa - 1} \cdot \dot{Q}_A \cdot p_1 \cdot \left[\left(\frac{p_2}{p_1} \right)^{\frac{\kappa-1}{\kappa}} - 1 \right] \tag{4.3}$$

The ratio p_2/p_1 is the ratio between exit pressure (p_2) and inlet pressure (p_1). These pressures are absolute pressures. Results of calculations for a typical site screw compressor are displayed in Fig. 4.4. It can be seen from the plotted lines that the relationship between pressure ratio and power rating has a degressive trend. The relative power consumption is lower at the higher pressure ratios.

The theoretical power of the compressor type XAHS 365 in Table 4.1, estimated with (4.3), has a value of $P_H = 130\,\text{kW}$. In practice, the theoretical power input is just a part of the actual power, transmitted through the compressor coupling. The actual power should include dynamic flow losses and mechanical losses. Therefore, the actual power of a compressor reads as follows:

$$P_K = \eta_{Km} \cdot \eta_{Kd} \cdot P_H \tag{4.4}$$

The mechanical losses, typically amounting to 8–12% ($\eta_{Km} = 0.08$–0.12) of the actual power, refer to viscous or frictional losses due to the bearings, the timing and step-up gears. The dynamic losses typically amount to 10–15% ($\eta_{Kd} = 0.1 - 0.15$)

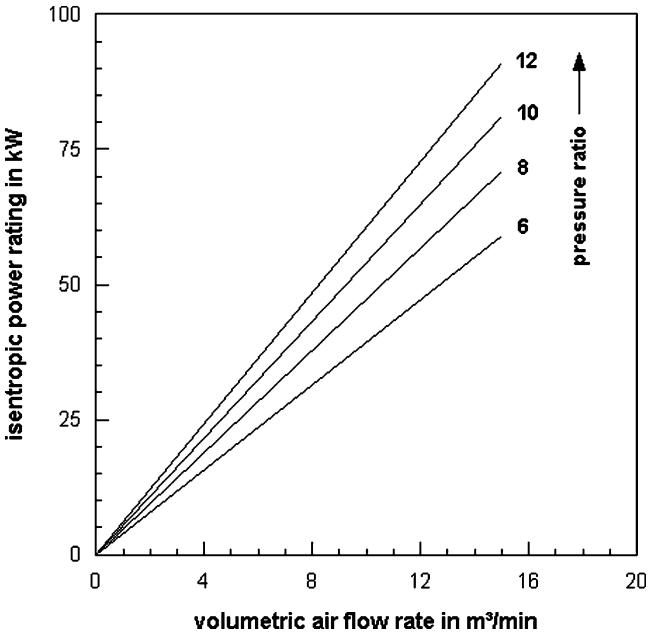

Fig. 4.4 Calculated compression power values, based on (4.3)

of the actual power. More information on these issues can be found in Bloch (1995) and Grabow (2002). The actual power rating of the compressor type XAHS 365 in Table 4.1 is P_K = 206 kW. If the theoretical power of P_H = 130 kW, estimated with (4.3), is related to this value, the losses cover about 36%.

Air compressors can be evaluated based on their specific power consumption, which is defined as the ratio between actual power rating and volumetric air flow rate:

$$P_S = \frac{P_K}{\dot{Q}_A} \tag{4.5}$$

For the compressor type XAHS 365 in Table 4.1, the specific power consumption is, for example, $P_S = 9.6\,\text{kW}/(\text{m}^3/\text{min})$. Different types of compressors have different specific power consumptions even if they deliver equal pressure and volumetric air flow rate values. Larger compressors have lower specific power consumption; thus, they perform more efficient. The physical unit of the specific power consumption is that of a specific volumetric energy (kWh/m^3), and it can, therefore, also characterise the energy required for the compression of a given air volume.

Part of the compression energy is consumed by the heating of the gas. Gas temperature increases during the compression process. For an adiabatic compression process, the final gas temperature can be calculated with the following equation (Bendler, 1983):

$$T_K = T_1 \cdot \left(\frac{p_2}{p_1}\right)^{\frac{\kappa-1}{\kappa}} \tag{4.6}$$

Results of calculations are displayed in Fig. 4.5. It can be seen that air temperatures as high as $\vartheta = 300^\circ\text{C}$ can be achieved. Because hot air can carry much more moisture than cold air, there is a high risk of condensation in the blast cleaning system. More detailed information on this issue is presented, among others, by Siegel (1991). This author provides a nomogram where the amount of condensation water can be read for different pressure ratios. A typical calculation example ($p_2 = 0.6\,\text{MPa}$, $\vartheta_1 = 20^\circ\text{C}$, 60% relative humidity) delivers a condensation water rate of 8 g per cubic metre of air. For a volumetric air flow rate of $\dot{Q}_A = 10\,\text{m}^3/\text{h}$, the total amount of condensation water would be about 5 l/h. Therefore, an after cooling process is recommended after the compression process.

4.2.4 Economic Aspects

The technical and economical evaluation of compressors is a complex issue. However, the key performance parameters, pressure (p) and volumetric air flow rate ($\dot{Q}_A$), usually allow a selection of appropriate consumers (e.g. grinders and blast cleaning nozzles). Key roles in the interaction between compressor and air consumers not only play dimension and condition of the consumers, in particular blast cleaning nozzles (see Fig. 4.3); but also the dimensions of connecting devices,

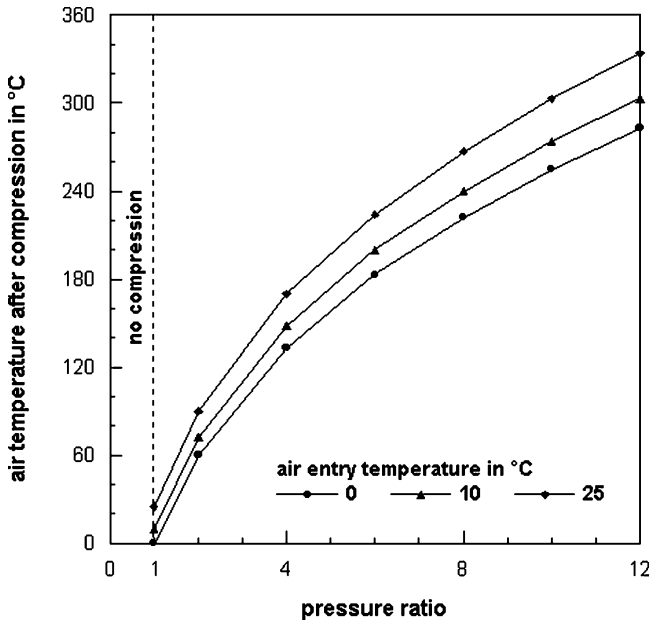

Fig. 4.5 Calculated air exit temperature after adiabatic compression; based on (4.6)

in particular hose lines, valves and fittings. If these parts are insufficiently tuned, efficiency drops and costs increase. These aspects are discussed in the following sections.

Pressure losses in hoses, fittings and armatures as well as leakages must also be taken into account if the size of a compressor needs to be estimated. This aspect is discussed in Sects. 4.4 and 4.5.

Another problem is pressure fluctuation, which affects the volumetric air flow rate. A rule says that even good maintained compressors require a correction factor of 1.05. This means a plus of +5% to the nominal volumetric flow rate requested by the consumer.

The pressure valve located at the outlet of the compressors should be adjusted to the nozzle diameter of the blast cleaning system. Some relationships are listed in Table 4.2. A general recommendation is as follows: $d_{VK} \geq 4 \cdot d_N$. For a nozzle with a diameter of $d_N = 10\,\text{mm}$, the minimal internal diameter of the compressor outlet valve should be $d_{VK} = 40\,\text{mm}$. Values for the sizes of air exit valves of three compressors are listed in Table 4.1.

A good maintenance programme is critical to compressor life and performance. A good maintenance programme is one that identifies the need for service based on time intervals and equipment hours. Additional items that also need to be considered when developing a programme are environmental conditions such as dust, ambient temperature and humidity, where filter changes may be required before the recommended intervals. Most equipment manufacturers have developed a preventive

Table 4.2 Adjustment between nozzle diameter and compressor outlet valve diameter (Clemco Inc., Washington)

Nozzle diameter in mm	Valve diameter in mm
5.0	19
6.5	25
8.0	32
9.5	38
11.0	50
12.5	50
16.0	64
19.0	76

maintenance schedule for their equipment, and it must be followed as a minimum. However, manufacturers cannot account for all operational conditions, and a maintenance plan may be developed by the operator of the equipment. Table 4.3 lists some recommendations.

4.2.5 Aspects of Air Quality

Basically, compressed air can be subdivided into the following four groups:

- oil-free air;
- moisture-free air;
- oil-lubricated air;
- breathing air.

Regulatory demands on the quality of pressurised air are prescribed in ISO 8573-1 (2001). The most important criteria are listed in Table 4.4. It can be seen that the standard distinguished between 10 quality classes for compressed air. Major assessment parameters include solid content (respectively dust), moisture content and oil content.

The requirement for oil-free air comes from surface quality arguments. The occupancy of blast cleaned steel surfaces by oil will reduce the adhesion of the coating systems to the substrate, and it will deteriorate the protective performance. These aspects are discussed in Sect. 8.4. In oil-injected compressors, the air usually picks up a certain amount of oil due to its way through the compaction room. This oil can appear as liquid, aerosol, or even as vapour. Even professionally maintained screw compressors ran without oil separators generate rest oil contents as high as 5 ppm (milligram of oil per cubic metre of air). Part of this oil will be intercepted together with condensation water in appropriate cooling devices. However, in order to also separate oil vapour reliably, multiple-step cleaning systems are required. A typical system consists of the following components:

- an after-cooler to cool down the compressed air;
- a high-performance fine filter to intercept aerosols;
- an activated carbon filter to absorb oil vapours.

Table 4.3 Example of a preventive air compressor maintenance programme (Placke, 2005)

	Daily	Weekly	Monthly	Quarterly	Bi-yearly	Yearly
Small size unit				250 h	500 h	1,000 h
Large size unit				500 h	1,000 h	2,000 h
Compressor oil level	C					
Engine oil level	C					
Radiator cooling level	C					
Meters/lamps	C					
Air filter service gauge	C					
Fuel tank (fill at shift end)	C				Empty	
Water/fuel separator empty	C					
Discharger of pre-cleaner of air cleaner		C				
Alternator belts		C				
Battery connections/level		C				
Tire pressure/tread		C				
Wheel bolts			C			
Hoses (oil, air, intake, etc.)			C			
Automatic shutdown system test			C			
Air purificator system, visual			C			
Compressor oil radiator, external			C	Clean		
Engine oil radiator, external			C	Clean		
Clamps				C		
Air purificator elements				W		
Fuel/water separator element					R	
Compressor element				B	A	
Compressor oil					R	
Wheels (bearings, seals, etc.)					C	C
Engine cooler tests					C	R
Shutdown switch lockout test						C
Scavenging orifice and common elements						Clean
Oil separator element						R
Hook Augen bolts	Check before towing					
Lights (drive, brakes, flasher)	Check before towing					
Engine oil change, filters, etc.	Refer to the engine operators manual					

A – Change only to the small size unit; B – Change only to the large size unit; C – Check (adjust or replace as needed); R – Replace; WI – When indicated

Moisture-free compressed air is recommended for blast cleaning operations to avoid moisturisation of abrasive particles. Moist particles tend to agglutinate which could, in turn, clog pressure air lines. Many compressors are equipped with devices that remove condensation water. These devices include the following parts:

- an after-cooler;
- a condensation water precipitator;
- a filter systems to separate water vapour;
- an air heating systems.

There are also anti-icing lubrication agents available that can absorb water and reduce the hazard of ice formation.

Table 4.4 Quality classes for compressed air (ISO 8573-1)

Class	Solids/dust							
	Max. number per m^3 of particles with given diameter				Size in µm	Content in mg/m^3	Moisture Pressure dew point in °C (X_W = water in g/m^3)	Total oil content in mg/m^3
	≤ 0.1	$0.1 < 0.5$	$0.5 < 1.0$	$1.0 < 5.0$				
0	According to operator							
1	–	100	1	0	–	–	≤ -70	$\leq$0.01
2	–	100,000	1,000	10	–	–	≤ -40	$\leq$0.1
3	–	–	10,000	500	–	–	≤ -20	$\leq$1.0
4	–	–	–	1,000	–		$\leq +3$	$\leq$5.0
5	–	–	–	20,000	–	–	$\leq +7$	–
6	–	–	–	–	$\leq$5	$\leq$5	$\leq +10$	–
7	–	–	–	–	$\leq$40	$\leq$10	$X_W \leq 0.5$	–
8	–	–	–	–	–	–	$0.5 \leq X_W \leq 5.0$	–
9	–	–	–	–	–	–	$5.0 \leq X_W \leq 10.0$	–

Table 4.5 Limits for breathing air according to DIN 3188

Medium	Limit
Carbon dioxide	$<800\,mg/m^3$ air
Carbon monoxide	$<30\,mg/m^3$ air
Dust	Max. 0.01 µm
Oil vapour	$0.3\,mg/m^3$ (20°C and 0.7 MPa)

The supply of breathing air is especially important for all blast cleaning operations. Critical substances in breathing air include carbon dioxide, carbon monoxide, dust and oil vapour. Regulatory limits for breathing air are listed in Table 4.5. Compressed air without special treatment cannot meet these requirements. Therefore, compressed air needs to be treated in breathing air treatment devices. These devices usually perform in multiple steps, and they include fine filters to intercept water, oil and dust; activated carbon filters to adsorb oil vapour; and catalysts to strip carbon dioxide and carbon monoxide.

4.3 Blast Machine

4.3.1 Basic Parts

The blast machine is a key part of any dry blast cleaning configuration. The major task of the blast machine is the delivery and dosing of the abrasive particles into the air stream. The structure of a typical blast machine is shown in Fig. 4.6. It consists basically of an air inlet line, a pressure sealing system, the actual storage part and an abrasive metering system. Blast machines are available at numerous sizes.

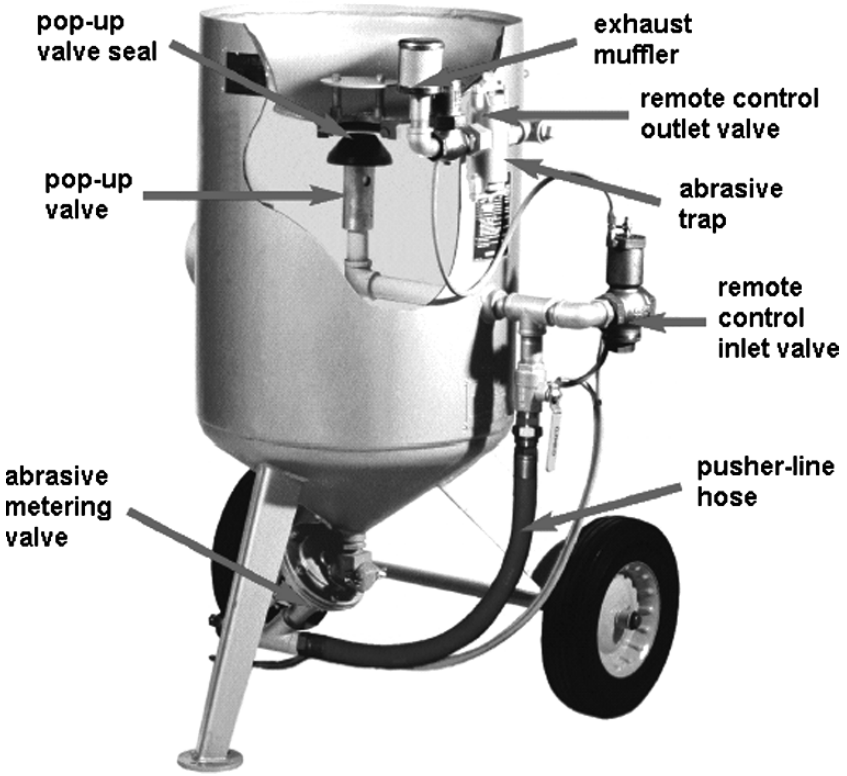

Fig. 4.6 Basic design of a blast pot (Clemco, Inc., Washington)

4.3.2 Abrasive Metering

4.3.2.1 Effects of Process Parameters

The metering of the abrasive particles is a challenging task, and the success of a blast cleaning operation depends to some amount on correct and reliable metering (see Sect. 6.4.1). The mass flow rate of abrasives is regulated simply due to changes in the size of the passage in a metering valve. Plaster's, (1972) review still gives a very good overview on typical pressure vessels and mixing valve designs. More recent information was provided by Nadkarni and Sharma (1996).

The performance of abrasive metering processes was investigated by Bae et al. (2007), Bothen (2000) and Remmelts (1968). The process of abrasive mass flow metering due to valve passage size variations is illustrated in Fig. 4.7, where the abrasive mass flow rate is plotted against the passage size for a given valve system. A power relationship with a power exponent greater unity can be noted between valve opening size and abrasive mass flow rate. The graphs also illustrate the effects of changes in nozzle diameter: the larger the nozzle, the more abrasive material was pushed through the valve passage. Changes in nozzle diameter seemed to affect the

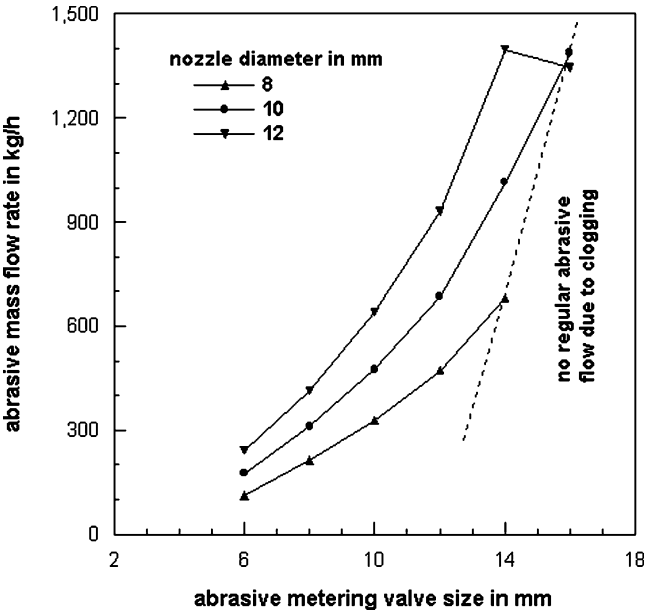

Fig. 4.7 Effects of metering valve passage and nozzle diameter on abrasive mass flow rate (Remmelts, 1968). Air pressure: $p = 0.5$ MPa; abrasive type: Zirconium; abrasive size: $d_p = 100\,\mu m$

abrasive mass flow rate, especially, at the large valve openings. The diameter of the blast cleaning nozzle seemed to influence the power exponents for the individual graphs. The larger the nozzle diameter, the higher was the value for the power exponent. A critical case is illustrated in Fig. 4.7 by the divergent process behaviour for the largest valve opening – here, a clogging of the abrasive material can be noted. The cross-section of the valve opening was too small to maintain the abrasive delivery process if the abrasive mass flow rate exceeded a value of about $\dot{m}_P = 24$ kg/min. Therefore, valve size and nozzle diameter must always be adjusted accordingly.

Effects of air volume flow rate on the abrasive metering process are shown in Figs. 4.8 and 4.9. There is a general trend that abrasive mass flow rate increased if air volume flow rate increased, but the detailed situation is very complex. In the case of the lower air pressure ($p = 0.4$ MPa) in Fig. 4.8, the metering process seemed to become very unstable at high air volume flow rates. It may be considered that the situation shown in Fig. 4.8 applies to micro-blasting processes, which involve very small abrasive particles as well as rather small dimensions for the metering device. A precise abrasive metering process could not be maintained under these special conditions.

Abrasive metering is also sensitive to changes in air pressure. The higher the pressure, the more abrasive material is pushed through the valve passage (Goldman et al., 1990; Mellali et al., 1994; Bothen, 2000; Remmelts, 1968). Examples are shown in Figs. 4.8 and 4.10. Mellali et al. (1994) performed measurements with

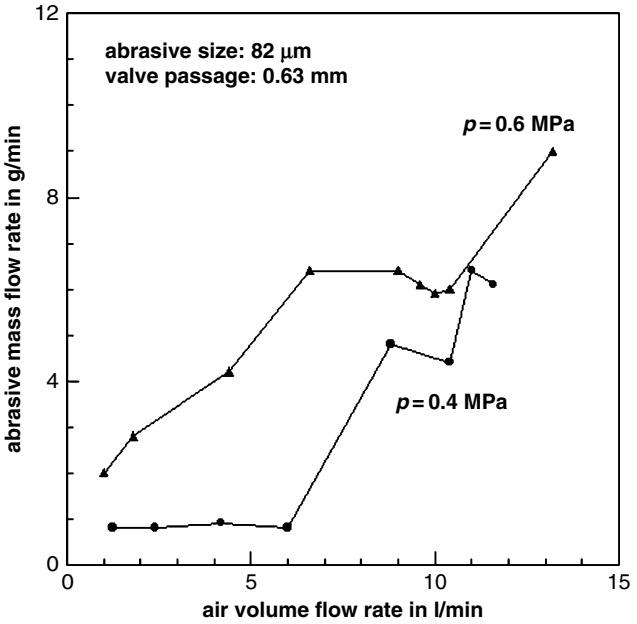

Fig. 4.8 Effects of air volumetric flow rate and pressure on abrasive mass flow rate (Bothen, 2000)

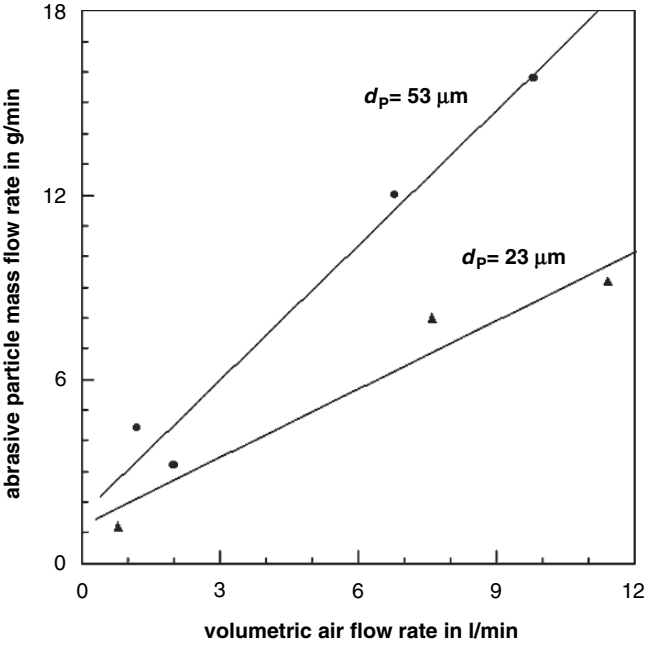

Fig. 4.9 Effects of air volumetric flow rate and abrasive particle size on abrasive mass flow rate for a micro-blasting machine (Bothen, 2000)

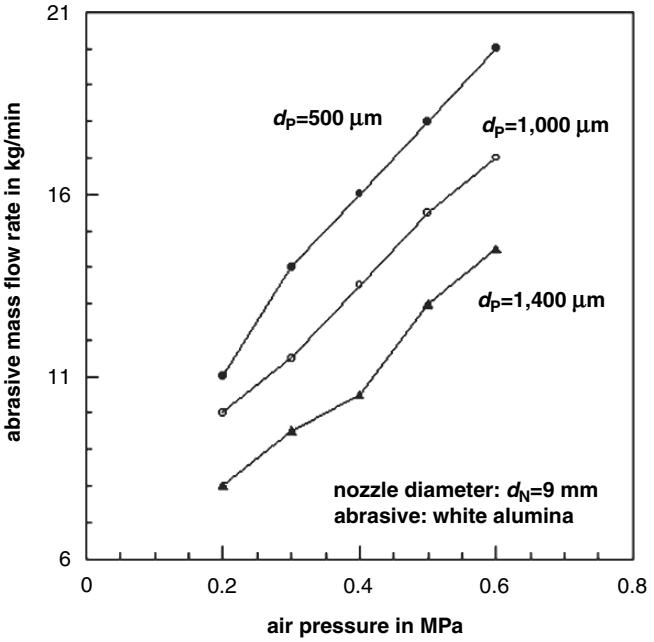

Fig. 4.10 Effects of air pressure and abrasive particle size on abrasive mass flow rate (Mellali et al., 1994)

aluminium oxide abrasives ($d_P = 500$–$1{,}400$ µm), and they found an almost linear relationship between air pressure and abrasive mass flow rate delivered by a laboratory blast pot. Results of their work are provided in Fig. 4.10. It can be seen that the functional relationships between both parameters followed a linear trend and that ascents of the functions depended on the abrasive particle size. The steepest ascent was estimated for the smallest abrasive particle diameter. The difference in abrasive mass flow rate in the parameter range considered in Fig. 4.10 was as high as 300%. Stallmann et al. (1988) measured the abrasive mass flow rate for two slag materials at three different compressor pressure levels, and they noted rather complex relationships as well as abrasive type effects. Whereas abrasive mass flow rate increased with an increase in the compressor pressure for copper slag, it showed maximum values at a moderate compressor pressure for melting chamber slag.

Effects of abrasive particle size variations on the performance of abrasive metering processes were investigated by Bothen (2000), Goldman et al. (1990) and Mellali et al. (1994). It was shown by Mellali et al. (1994) that abrasive mass flow rate delivered by a metering valve arrangement was very sensitive to changes in abrasive particle size. Results are provided in Fig. 4.10. It can be seen that abrasive mass flow rate increased if smaller abrasive particles were added to the system. This trend was also found for the use of glass beads by Goldman et al. (1990), whereby the effect of abrasive size seemed, however, to become insignificant at rather low pressures ($p < 0.2$ MPa). For the highest pressure ($p = 0.6$ MPa) in Fig. 4.10, the

difference in abrasive mass flow rate, caused by changes in the abrasive particle size, was as high as 40%. Another example for the influence of the abrasive particle size on abrasive mass flow rate is depicted in Fig. 4.9. In that particular case, the abrasive mass flow rate delivered by the metering system was larger for the larger abrasive particle diameters at a given valve passage size. This result does not agree with the results delivered by Goldman et al. (1990) and Mellali et al. (1994). A reason could be the very small dimensions for the abrasive materials ($d_P = 23$–$53\ \mu m$) and the valve ($d_V = 670$–$1{,}000\ \mu m$) used by Bothen (2000).

Adlassing and Jahn (1961) reported on measurements on the effects of abrasive material density and abrasive bulk density on the abrasive mass flow rate delivered by an abrasive metering device. These authors could prove that the abrasive mass flow rate increased almost linearly with an increase in the abrasive material density. The progress of the linear functions was independent of nozzle pressure ($p = 0.2$–$0.4\,MPa$). The lowest abrasive mass flow rate was measured for quartz sand ($\rho_P = 2{,}600\,kg/m^3$; $\rho_B = 1.48\,kg/l$), and the largest abrasive mass flow rate was measured for steel cut wire ($\rho_P = 7{,}900\,kg/m^3$; $\rho_B = 4.29\,kg/l$).

Figure 4.11 illustrates the effects of nozzle layout and number of valve turns on the abrasive metering process. It can be seen that the geometry of the nozzle affected the metering process mainly in the range of high numbers of valve turns. However, the general linear trend between number of valve turns and mass ratio abrasive/air did not seem to be affected by variations in the nozzle geometry. Changes in nozzle geometry have an influence on both air mass flow rate and abrasive mass flow rate. It can be seen that the mass flow ratio abrasive/air took very high values for all numbers of valve turns; it was basically larger than a value of $\dot{m}_P/\dot{m}_A = 2$, which is an upper limit for an efficient blast cleaning process (see Sect. 6.4.1). The increase in the mass flow ratio abrasive/air is not only attributed to a larger amount of abrasive flowing through the larger valve opening, but is also due to a reduction in the volumetric air flow rate. This aspect is illustrated in Fig. 4.12. The higher the number of valve turns, the lower is the volumetric air flow rate measured at the nozzle. Figure 3.11 clarifies the problem from the point of view of abrasive mass flow rate. The trends are equal to those shown in Fig. 4.12. The geometry of the nozzle had a pronounced effect on the absolute values for the volumetric air flow rate, but it did not affect the general trends of the curves. If (3.11) and (3.15) are applied, the volumetric air flow rate at the nozzle can be calculated. For the conditions in Fig. 4.12 (assumed air temperature $\vartheta = 25^\circ C$), the following values were calculated: nozzle "1" ($d_N = 11.5\,mm$): $\dot{Q}_A = 8.2\,m^3/min$; nozzle "2" ($d_N = 11\,mm$): $\dot{Q}_A = 7.4\,m^3/min$ and nozzle "3" ($d_N = 12.5\,mm$): $\dot{Q}_A = 9.6\,m^3/min$. The amount of displaced air volume depended on number of valve turns, respectively on abrasive mass flow rate; but it could be as high as 50% for the conditions in Fig. 4.12 (for nine valve turns). If, however, the more typical condition of four valve turns is applied, the amount of displaced air volume is between 17% and 25%. These values approve results of measurements performed by other authors (see Sect. 3.2.1).

An increase in the number of valve turns increases the abrasive mass flow rate. An increase in mass flow rate will increase pressure drop in the grit hose, thus reducing the nozzle pressure. This effect is shown in Fig. 4.13. It can be seen that the air

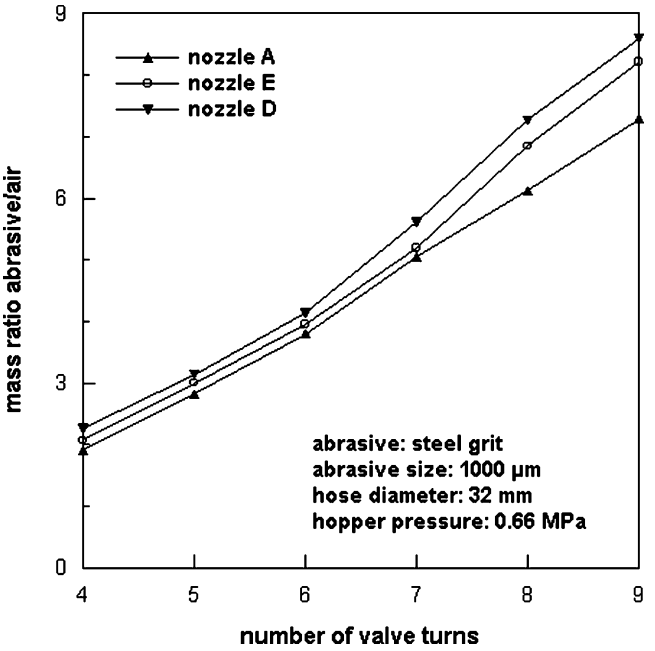

Fig. 4.11 Effects of number of valve turns and nozzle geometry on the mass flow ratio abrasive/air in convergent-divergent nozzles (Bae et al., 2007). Nozzle "A" – nozzle length: 125 mm, throat (nozzle) diameter: 12.5 mm, divergent angle: 7.6°, convergent angle: 3.9°; Nozzle "D" – nozzle length: 185.7 mm, throat (nozzle) diameter: 9.5 mm, divergent angle: 1.2°, convergent angle: 8.5°; Nozzle "E" – nozzle length: 215 mm, throat (nozzle) diameter: 11 mm, divergent angle: 1.3°, convergent angle: 7.9°

pressure at the nozzle dropped if abrasive mass flow rate increased. The pressure drop again depended on the geometry of the nozzle. It was most pronounced for the nozzle "A". For a typical value of $\dot{m}_P = 15\,\text{kg/min}$, the air pressure dropped from $p = 0.66\,\text{MPa}$ (at the hopper) down to $p = 0.53\,\text{MPa}$ at the nozzle if a grit hose with a diameter of $d_H = 32\,\text{mm}$ was used (hose length was not given). This particular problem will be discussed in more detail in Sect. 4.5.3.

The graphs in Fig. 4.11 illustrate another permanent problem in abrasive metering. The values for the mass ratio abrasive/air were very high if the number of valve turns was high. Mass ratios of $R_m = 1.0$–2.0 are most efficient for an effective blast cleaning (see Sect. 6.4.1). This optimum range was met for the arrangement in Fig. 4.11 for four valve turns only. Any additional valve turn will deteriorate the blast cleaning process although more abrasive mass is being delivered to the cleaning point.

4.3.2.2 Metering Models

The aforementioned relationships can be summarised as follows:

$$\dot{m}_P = f(d_V;\, d_N;\, p;\, d_P;\, \rho_P;\, \rho_B) \tag{4.7}$$

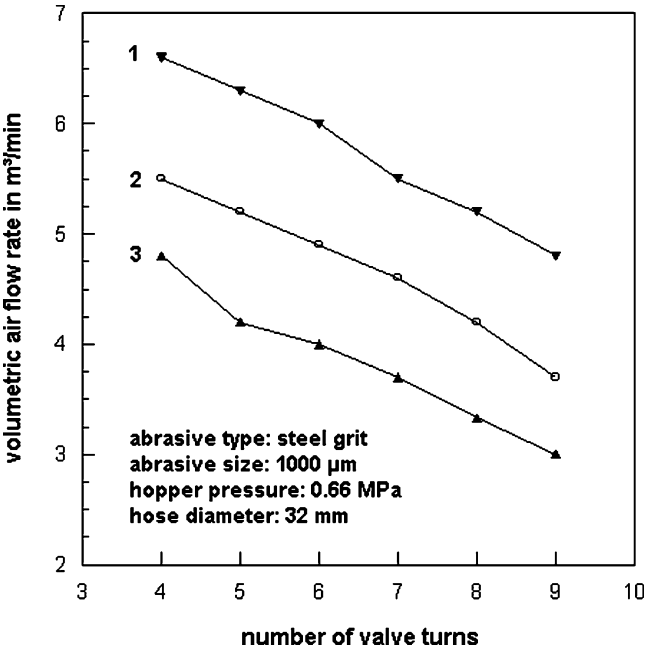

Fig. 4.12 Effects of number of valve turns and nozzle geometry on the volumetric air flow rate in convergent-divergent nozzles (Bae et al., 2007). Nozzle "1" – nozzle length: 150 mm, throat (nozzle) diameter: 9.5 mm, divergent angle: 2.1°, convergent angle: 9.3°; Nozzle "2" – nozzle length: 216 mm, throat (nozzle) diameter: 11.0 mm, divergent angle: 1.3°, convergent angle: 7.9°; Nozzle "3" – nozzle length: 125 mm, throat (nozzle) diameter: 12.5 mm, divergent angle: 7.6°, convergent angle: 3.9°

This complex relationship makes it almost impossible to reliably precalculate a certain desired abrasive mass flow rate.

Brauer (1971) reviewed the results of experimental investigations in the field of bulk material transport, and he suggested the following relationships:

$$\dot{m}_P \propto d_V^{2.5 \text{ to } 2.96} \tag{4.8a}$$

$$\dot{m}_P \propto d_P^{-0.18 \text{ to } -1.0} \tag{4.8b}$$

$$\dot{m}_P \propto \rho_P \tag{4.8c}$$

The qualitative trends between abrasive mass flow rate and valve opening size (Fig. 4.7), particle density and particle size (Fig. 4.10), which were discussed earlier, are properly reflected by these relationships.

Beverloo et al. (1961) developed a model for the approximation of the mass flow rate of particulate solids flowing through the discharge openings of hoppers. The model considers gravity-induced discharge only, and it is valid for particle sizes

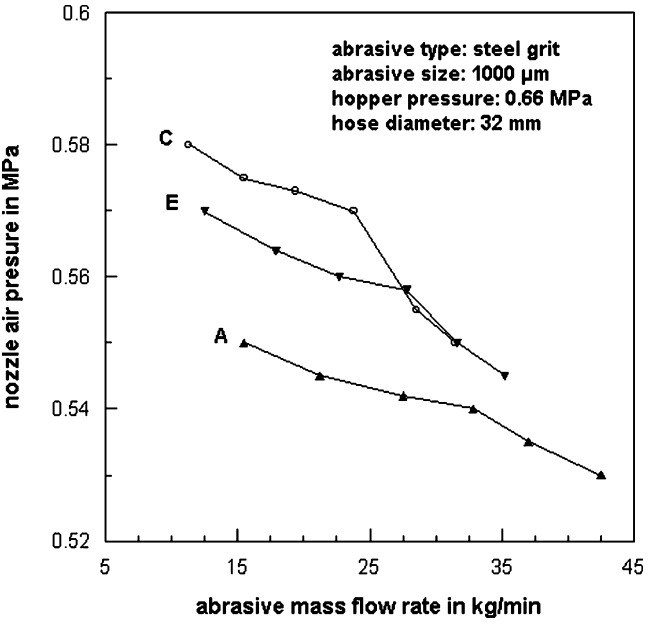

Fig. 4.13 Effects of abrasive mass flow rate and nozzle geometry on the nozzle air pressure (Bae et al., 2007). Nozzle "A" – nozzle length: 150 mm, throat (nozzle) diameter: 11.5 mm, divergent angle: 2.1°, convergent angle: 9.3°; Nozzle "C" – nozzle length: 125 mm, throat (nozzle) diameter: 12.5 mm, divergent angle: 7.6°, convergent angle: 3.9°; Nozzle "E" – nozzle length: 216 mm, throat (nozzle) diameter: 11.0 mm, divergent angle: 1.3°, convergent angle: 7.9°

larger than $d_P = 500$ µm. Another restriction is $d_V/d_P > 6$. The model delivers the following relationship:

$$\dot{m}_P \propto \rho_P \cdot g^{1/2} \cdot (d_V - k_Z \cdot d_P)^{5/2} \tag{4.9}$$

The parameter k_Z characterises the limit for gravity-induced flow. If pressure gradients are involved in the discharge process, a second term must be added, which leads to the following expression (Seville et al., 1997):

$$\dot{m}_P \propto \underbrace{\rho_P \cdot g^{1/2} \cdot (d_V - k_Z \cdot d_P)^{5/2}}_{\text{gravity induced}} \cdot \underbrace{\left(1 + \frac{\Delta p}{\rho_P \cdot g}\right)}_{\text{pressure gradient induced}} \tag{4.10}$$

The power relationship between mass flow rate and valve opening is clearly expressed in this relationship (see Fig. 4.7). The general trend for the effect of variations in particle size is also recorded, at least for standard dimensions of particles and valve opening (see Fig. 4.10). The proposed linear trend between abrasive material density and abrasive mass flow rate is supported by experimental results reported by Adlassing and Jahn (1961).

In practice, however, a working characteristic, similar to the graphs shown in Figs. 4.7 and 4.11, must be installed for any particular valve type for certain air pressures, nozzle diameters and abrasive materials. Such working characteristics are not available from manufacturers, and it must be estimated experimentally.

4.3.2.3 Abrasive Mass Flow Adjustment

In current industry practice, it is often the potman, who does this adjustment manually. How sensitive the entire blast cleaning procedure reacts on such a manual adjustment is illustrated in Fig. 6.20 and Table 4.6. Figure 6.20 shows that the cleaning rate was very sensitive to the number of turns for a metering valve. If the copper slag was being considered, a change from five turns to six turns led to an increase in cleaning rate from about 60 m^2/h to 72 m^2/h (+20%). The results listed in Table 4.6 illustrate the effects of manual fine adjustment on the blast cleaning process. If the number of turns of the metering valve was changed from 2 to 2.5 for garnet, cleaning rate almost tripled, and the specific abrasive consumption dropped up to –30%. For the steel grit, the situation was different. A change in the number of valve turns from 3 to 3.5 did not affect the cleaning rate, but increased the specific abrasive consumption by +30%. These examples highlight the economic potential of a precise abrasive metering.

Table 4.6 Metering valve adjustment test data (Hitzrot, 1997)

Abrasive material	Number of turns	Abrasive mass flow rate in kg/min	Cleaning rate in m^2/h	Specific abrasive consumption in kg/m^2
Fine coal slag	2	7.6	30.4	15.2
	3	9.5	32.4	17.7
	5	12.6	23.0	32.9
Star blast	2	5.5	24.3	13.6
	3	13.9	38.1	22.2
	5	17.5	36	29.3
Aluminium oxide	2	6.4	11.6	32.9
	3	13.0	19.4	40.0
	5	32.1	30.4	62.7
G-50 steel grit	2	5.4	11.3	28.3
	3	13.7	20.0	41.4
	3.5	17.3	19.2	54.1
	4.5	19.7	19.7	59.6
Garnet	2	2.6	6.6	23.8
	2.5	5.6	19.6	17.2
	3	10.1	20.9	28.8
	3.5	10.6	21.1	30.8
	4.5	21.3	23.7	54.1
Glass blast	2.75	7.6	19.3	23.8
	3	10.0	22.5	26.8
	3.5	11.5	29.9	22.7
	4	18.1	29.9	36.4

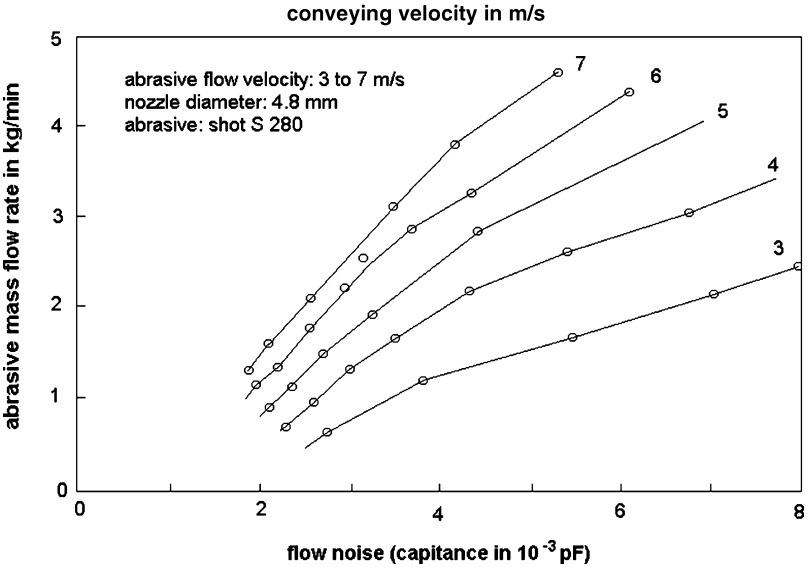

Fig. 4.14 Relationship between abrasive mass flow rate, abrasive conveying velocity in an abrasive hose, and the flow noise (Neelakantan and Green, 1982)

An experienced potman adjusts the abrasive mass flow rate according to the noise developed by the abrasive material if it flows through the hose. An optimum flow pattern causes a typical noise (see Sect. 4.5.1 for flow pattern types). Results plotted in Fig. 4.14 show that this empirical approach has a physical background. The flow noise had distinct relationships with air flow velocity in the hose and abrasive mass flow rate. These relationships offer the opportunity to control and adjust abrasive mass flow rates by acquiring and treating acoustic signals.

4.4 Pressure Air Hose Lines

4.4.1 Materials and Technical Parameters

The transport of the compressed air from the compressor to the blast machine occurs through pressure lines. For on-site applications, these are flexible hose lines. Hose lines are actually flexible hoses operationally connected by suitable hose fittings. Hose fittings are component parts or sub-assemblies of a hose line to functionally connect hoses with a line system or with each other. Pressure air hoses are flexible, tubular semi-finished product designed of one or several layers and inserts. They consist of an outer cover (polyamide, nylon), a pressure support (specially treated high-tensile steel wire) and an inner core (POM, polyamide, nylon). Technical parameters are listed in Table 4.7. It can be recognised from the listed values that the hose diameter is an important handling parameter. An increase in hose diameter is

Table 4.7 Technical parameters for blast cleaning hoses (Phoenix Fluid Handling Industry GmbH, Hamburg)

Internal diameter in mm	Wall thickness in mm	Bend radius in mm	Specific weight in kg/m
19	5.0	95	0.95
25	7.0	125	1.00
32	8.0	200	1.38
38	8.0	240	1.60
42	9.0	330	2.00

accompanied by an increase in bend radius and an increase in specific weight. Thus, larger hoses are more difficult to handle.

4.4.2 Air Hose Diameter Selection

The speed of the air flow through the hose for compressible flow can be calculated based on mass flow conservation, which delivers the following relationship:

$$v_F = \frac{4}{\pi} \cdot \frac{\dot{m}_A}{\rho_A \cdot d_H^2} \tag{4.11}$$

The air density, and therefore the flow velocity, depends on pressure and temperature [see (3.6)]. Typical hose diameters for blast cleaning operations are between $d_H = 19\,\text{mm}$ and 50 mm (see Table 4.7). For a volumetric flow rate of $\dot{Q}_A = 10\,\text{m}^3/\text{min}$, delivered at a pressure of $p = 1.0\,\text{MPa}$, the velocity of the air flow for a hose diameter of $d_H = 40\,\text{mm}$ is $v_F = 13\,\text{m/s}$. More results of calculations are provided in Fig. 4.15.

An empirical rule for selecting the proper hose diameter is: the flow velocity in the hose should not exceed the value of $v_F = 15\,\text{m/s}$ (Gillessen et al., 1995). Based on (4.11), the corresponding minimum hose diameter is as follows:

$$d_H = 0.29 \cdot \left(\frac{\dot{m}_A}{\rho_A(p, T)} \right)^{1/2} \tag{4.12}$$

In that equation, the air mass flow rate is given in kg/s, and the hose diameter is given in m. If no standard diameter is available for the calculated value, the next larger diameter should be selected. As an example, for an air mass flow rate of $\dot{m}_A = 10\,\text{kg/min}$, delivered at a pressure of $p = 1.0\,\text{MPa}$ and a temperature of $\vartheta = 20^\circ\text{C}$, (4.12) delivers a value of $d_H = 34.5\,\text{mm}$; the recommended internal hose diameter is $d_H = 38\,\text{mm}$. The critical hose diameters for the situations displayed in Fig. 4.15 are: $d_H = 45\,\text{mm}$ for $p = 0.7\,\text{MPa}$; $d_H = 40\,\text{mm}$ for $p = 0.9\,\text{MPa}$ and $d_H = 37\,\text{mm}$ for $p = 1.1\,\text{MPa}$. The lower the pressure, the higher becomes the selected hose diameter. The reason is the increase in volumetric air flow rate if the air pressure drops [see (3.1)]. For a given air volumetric flow rate, the trend between air pressure and critical hose diameter follows

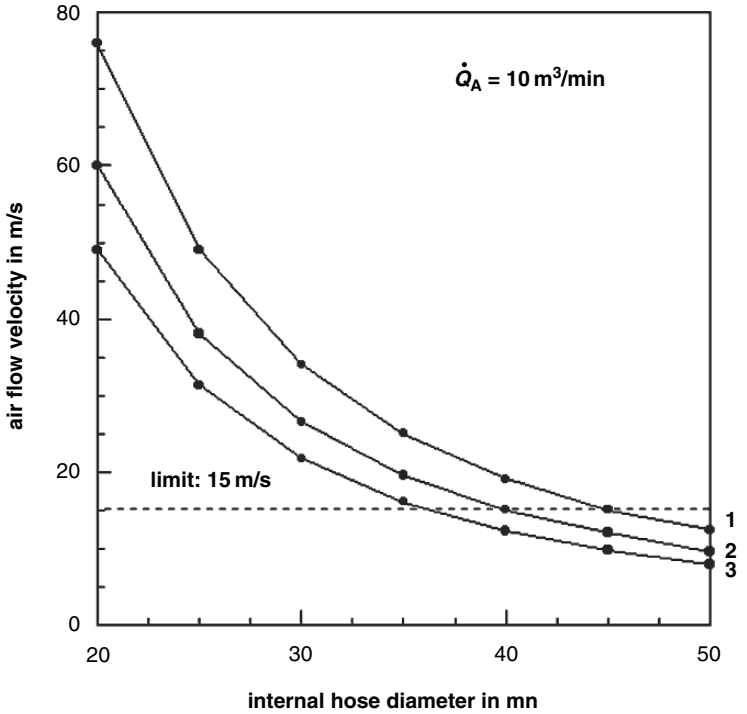

Fig. 4.15 Calculated air flow velocities in blast cleaning air hoses (air flow rate: $\dot{Q}_A = 10\,m^3/min$). Pressure levels: "1" – $p = 0.7$ MPa; "2" – $p = 0.9$ MPa; "3" – $p = 1.1$ MPa

a power relationship with a negative power exponent (for the examples in Fig. 4.15, the power exponent has a value of –0.43).

4.4.3 Pressure Drop in Air Hose Lines

4.4.3.1 General Approach

A permanent problem with air hose lines is the pressure drop in the hose lines. The situation is illustrated in Fig. 4.16. The well-known general approach for estimating the pressure drop for incompressible flow is as follows (Bohl, 1989):

$$\frac{\Delta p_A}{\rho_A} = \underbrace{\sum_i \left(\lambda_{Ai} \cdot \frac{l_H}{d_H} \cdot \frac{v_F^2}{2}\right)}_{\text{straight hose}} + \underbrace{\sum_k \left(\xi_{Ak} \cdot \frac{v_F^2}{2}\right)}_{\text{knees and aramtures}} \tag{4.13}$$

$$\Delta p_A = p_1 - p_2$$

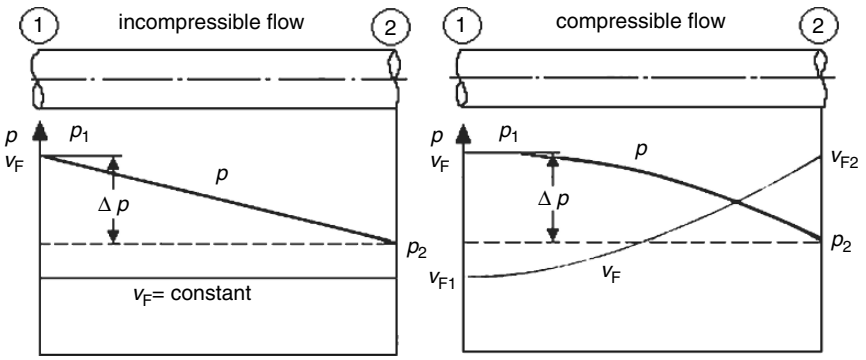

Fig. 4.16 Parameter variation along a hose line for compressible flow conditions (adapted from Wille, 2005)

where, p_1 is the static pressure at the point "1" and p_2 is the static pressure at the point "2" as shown in Fig. 4.16. The parameters λ_A and ξ_A are friction numbers, v_F is the flow velocity, l_H is the hose length, and d_H is the hose diameter.

However, for compressible flow, which should usually be considered for the air flow in blast cleaning hoses, the pressure drop is not linear, and the air flow velocity is not at a constant level over the hose length (see Fig. 4.16, right drawing). Approximations for the calculation of pressure losses for compressible flow can be found in standard monographs on technical fluid dynamics (Glück, 1988; Bohl, 1989; Sigloch, 2004). A feasible approximation is as follows (Bohl, 1989):

$$\frac{p_1^2 - p_2^2}{2 \cdot p_1} = \lambda_A \cdot \frac{l_H}{d_H} \cdot \rho_A \cdot \frac{v_F^2}{2} \cdot \frac{\bar{T}}{T_1} \tag{4.14}$$

Here, the density variation over the hose length (due to changes in pressure and temperature) must be considered. The average temperature can be assumed as follows:

$$\bar{T} \approx \frac{T_1 + T_2}{2} \tag{4.15}$$

The temperature at the end of the hose line can be approximated as follows:

$$T_2 \approx T_1 \cdot \left(\frac{p_2}{p_1}\right)^{\frac{\kappa-1}{\kappa}} \tag{4.16}$$

If the temperature does not vary notably along the hose length (isotherm flow), the term $\bar{T}/T_1$ in (4.14) can be neglected. For an adiabatic flow, however, the temperature term must be considered.

4.4.3.2 Friction Numbers

The friction number for wall friction depends on the Reynolds number and on the ratio between hose diameter and internal wall roughness. The general relationship is as follows (Bohl, 1989):

$$\lambda_A = f\left(Re_H; \frac{k_H}{d_H}\right) \tag{4.17}$$

The Reynolds number of the air flow through a hose is given as follows:

$$Re_H = \frac{v_F \cdot d_H \cdot \rho_A}{\eta_A} \tag{4.18}$$

It can be seen that Re_H is a function of pressure and temperature, because density and dynamic viscosity of the air are involved in the calculations. In order to consider these effects, (3.6) and (3.7) must be applied. For a pressure of $p = 1.0\,\text{MPa}$, a volumetric flow rate of $\dot{Q}_A = 10\,\text{m}^3/\text{min}$, an air temperature of $\vartheta = 20^\circ\text{C}$ and a hose diameter of $d_H = 35\,\text{mm}$, the Reynolds number is $Re_H = 4.1 \times 10^5$. More results of calculations are provided in Fig. 4.17. It can be seen that changes in temperature have only marginal effects. The Reynolds number decreases if the hose diameter increases. A combination of (4.11) and (4.18) delivers the relationship: $Re_H \propto d_H^{-1}$.

The precise solution to (4.17) is a function of the flow type in the hose and the thickness of the laminar boundary layer at the hose wall. For blast cleaning processes, a turbulent flow ($Re_H > 2{,}300$) is basically assumed. However, even if the flow is turbulent, a thin laminar boundary layer forms at the wall regions of the hoses (Bohl, 1989; Wille, 2005). This laminar layer is illustrated in Fig. 4.18. The thickness of this layer can be calculated as follows (Wille, 2005):

$$\delta_H = \frac{5}{Re_H^{1/2}} \cdot d_H \tag{4.19}$$

Results of (4.19) are displayed in Fig. 4.19. It can be seen that air temperature does not have a notable effect on the thickness of the boundary layer. But the effect of the hose diameter is very pronounced. Combining (4.11), (4.18) and (4.19) delivers the relationship: $\delta_H \propto d_H^{3/2}$.

For $\delta_H > k_H$, the hose surface is considered to be *hydraulically smooth*, and the so-called Blasius equation can be utilised to calculate the friction number for a Reynolds number range between $Re_H = 2.3 \times 10^3$ and 10^5(Bohl, 1989):

$$\lambda_A = 0.3164 \cdot Re_H^{-0.25} \tag{4.20}$$

For higher Reynolds numbers between $Re_H = 10^5$ and 10^6, the so-called Nikuradse equation for hydraulically smooth pipes can be applied (Bohl, 1989):

$$\lambda_A = 0.0032 + 0.221 \cdot Re_H^{-0.237} \tag{4.21}$$

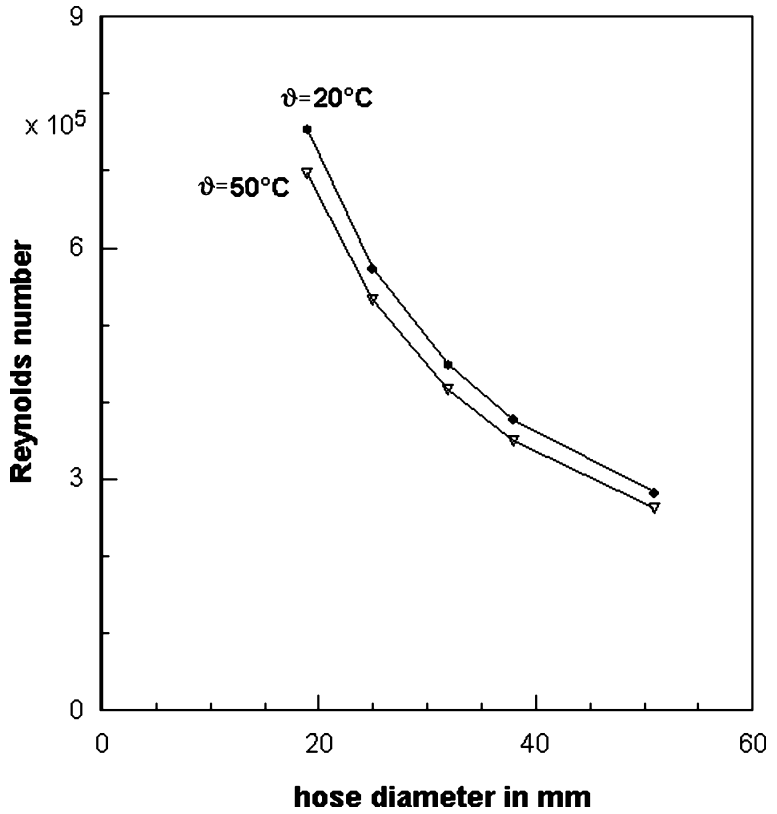

Fig. 4.17 Calculated Reynolds numbers for the flow of air in blast cleaning air hoses for two values of air temperature (air volume flow rate: $\dot{Q}_A = 10\,m^3/min$, air pressure: $p = 1.0\,MPa$)

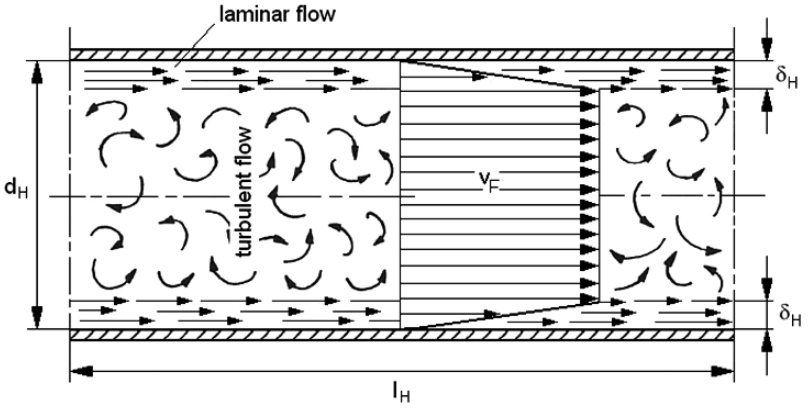

Fig. 4.18 Structure and parameters of a laminar boundary layer on a hose wall (Wagner, 1990)

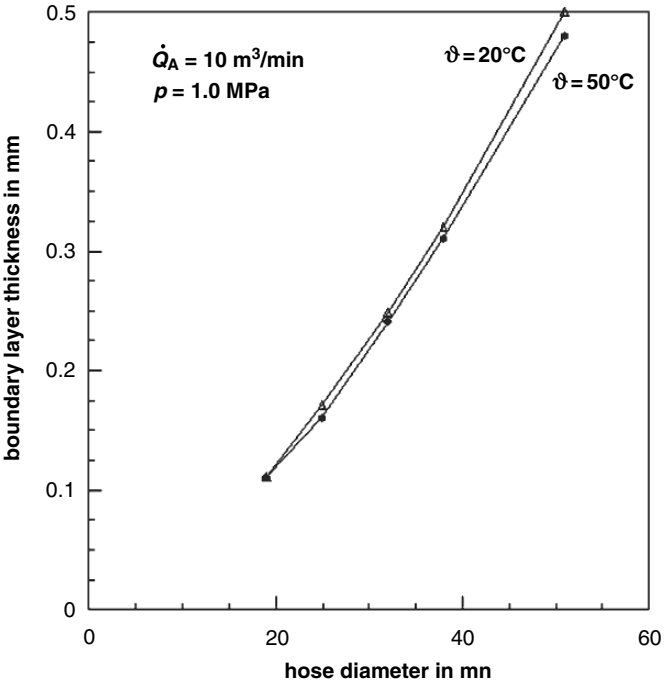

Fig. 4.19 Calculated values for the thickness of laminar boundary layers for the flow of air in blast cleaning hoses for two values of air temperature

In these cases, the friction number is independent of the wall roughness, and it is a function of the Reynolds number only. Equations (4.20) and (4.21) are graphically expressed in Figs. 4.20 and 4.21. Typical values for λ_A can be read from these two graphs.

For $\delta_H < k_H$, the hose surface is considered to be *hydraulically rough*, and the friction number can be estimated from the so-called Prandtl–Colebrook charts, which can be found in standard books on technical fluid mechanics (Oertel, 2001; Wille, 2005). A Prandtl–Colebrook chart is displayed in Fig. 4.22. If the Reynolds number and the ratio d_H/k_H are known, the corresponding value for λ_A can be read at the ordinate. The special case *hydraulically smooth* is also included in that graph. A general empirical relationship for the turbulent flow regime is the Colebrook-White equation (Wille, 2005):

$$\frac{1}{\lambda_A^{1/2}} = -2 \cdot \log \left(\frac{2.51}{Re_H \cdot \lambda_A^{1/2}} + 0.27 \cdot \frac{k_H}{d_H} \right) \tag{4.22}$$

Equations 4.20–4.22 are illustrated in Figs. 4.20–4.22. For the example mentioned above, the boundary layer thickness is $\delta_H = 0.27$ mm. Rubber hoses, manufactured for blast cleaning applications, have a typical roughness value of about

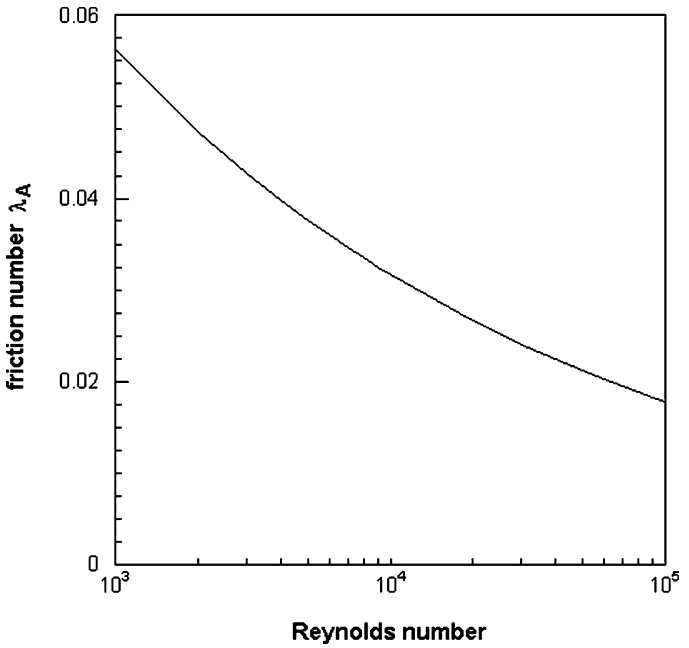

Fig. 4.20 Friction parameter for *hydraulically smooth* flow conditions at high Reynolds numbers: Blasius' solution (4.20)

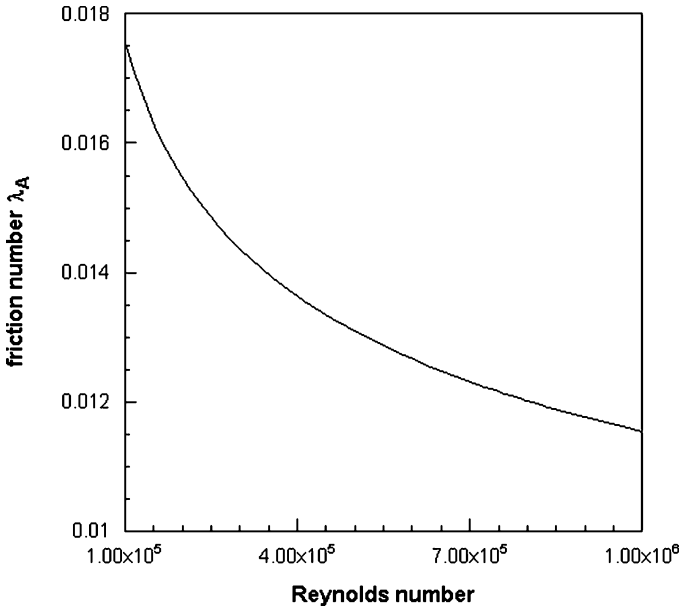

Fig. 4.21 Friction parameter for *hydraulically smooth* flow conditions at very high Reynolds numbers: Nikuradse's solution (4.21)

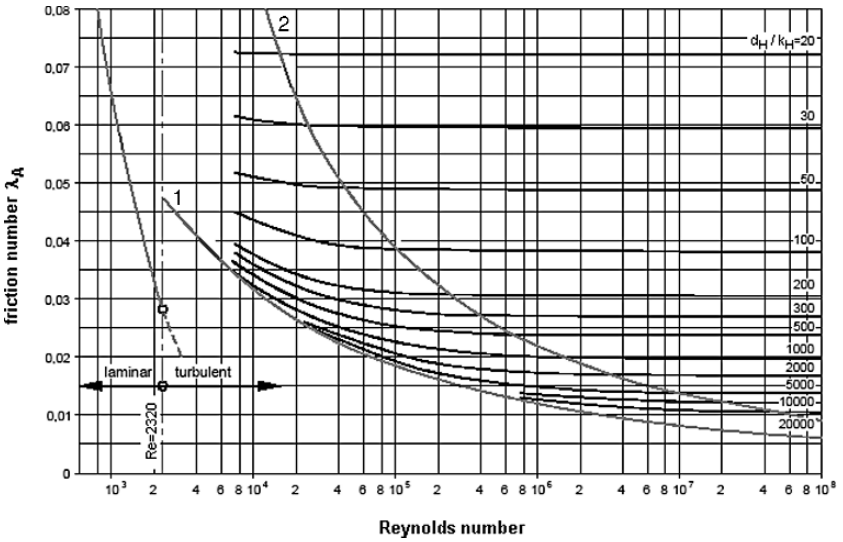

Fig. 4.22 Relationships between Reynolds number, relative roughness and friction parameter (Wille, 2005). 1-hydraulically smooth; 2-hydraulically rough (limit)

$k_H = 0.016\,mm$ (Bohl, 1989). This value is one order of magnitude lower than the typical values for the thickness of the laminar boundary layer (see Fig. 4.19). The Reynolds numbers for the flow in blast cleaning hoses usually exceed the value $Re_H = 10^5$ (see Fig. 4.17). Therefore, the rather simple (4.21) can be applied for the estimation of the friction number for most blast cleaning applications.

4.4.3.3 Hose Diameter Effects

The equations mentioned above deliver the following relationship between pressure drop and hose diameter:

$$\Delta p_A \propto d_H^{-5} \tag{4.23}$$

This equation illuminates the overwhelming influence of the hose diameter on the pressure loss. (A precise physical deviation delivers a power exponent value somewhat smaller than 5.) This influence is graphically expressed in Fig. 4.23, which shows results of measurements of the pressure drop in hoses with different diameters. The rapid pressure drop in the hose with the small diameter of $d_H = 19\,mm$ can be recognised. These experimental results agree very well with results calculated from (4.14). More values, calculated with (4.14), are plotted in Fig. 4.24. The graphs show, among others, that pressure drop reduces at higher air pressures. This phenomenon can be explained with (3.6), which suggests that the air density increases with an increase in pressure. Higher air density means lower air volume, which in turn reduces the air flow velocity in the hose. Equation 4.14 shows that lower air flow velocity leads to less pressure drop. More relationships are displayed in Fig. 4.16. The graphs show the relationship between hose length and air flow velocity in the

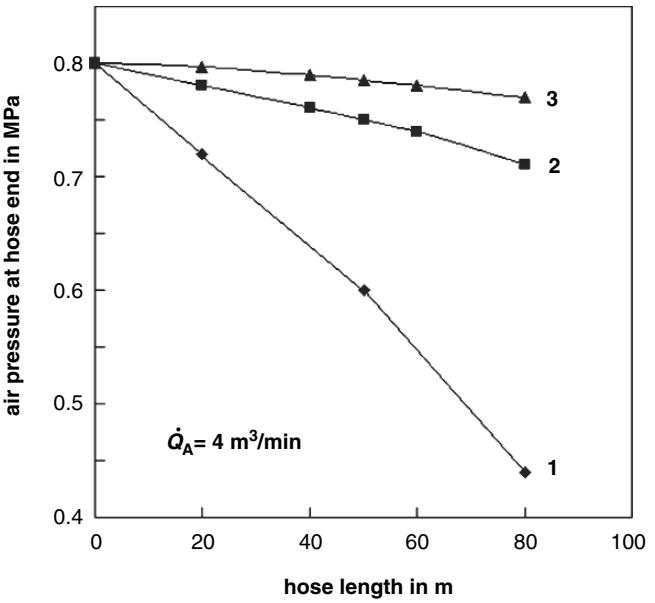

Fig. 4.23 Effect of hose diameter on experimentally estimated pressure loss in air hoses (Neumann, 1985). Air flow rate: $\dot{Q}_A = 4.0\,m^3/min$; hose diameter: "1" – $d_H = 19\,mm$; "2" – $d_H = 25\,mm$; "3" – $d_H = 32\,mm$. Pressure drop is non-linear

hose. It can be seen at the right graph in Fig. 4.16 that the air flow velocity increases with an increase in hose length. The reason is the expansion flow caused by the pressure drop in the hose line. Lower air pressure causes the air density to decrease. The reduction in air density leads to an increase in air volumetric flow rate and, thus, to an increase in flow velocity [see (4.11)]. Another important effect is that of the abrasive material. Although no abrasive material flows through the air hose, it affects the pressure drop. This effect is caused by the reduction in the air volumetric flow rate due to the addition of the abrasive particles [see (3.18) and Fig. 3.11].

4.4.3.4 Pressure Drop in Fittings and Armatures

The precise pressure drop in hose fittings and in armatures, characterised through ξ_A in (4.13), should be measured for any individual fitting. However, such values are not available for an individual accessory in most cases, but pressure loss values for certain groups and types of armatures and valves are published in the technical literature. A large collection of friction numbers for numerous armatures, valves, pipe elements, etc. can be found in Bohl's (1989) and Wagner's (1990) books. Two examples are shown in Figs. 4.25 and 4.26. For most valve constructions, the friction values are almost independent on pipe diameter. It can be seen that friction numbers for armatures are usually one order of magnitude larger than friction numbers for the flow in straight hoses. The valve constructions shown in Figs. 4.25 and 4.26, for example, can have friction numbers between $\xi_A = 1$ and 7.

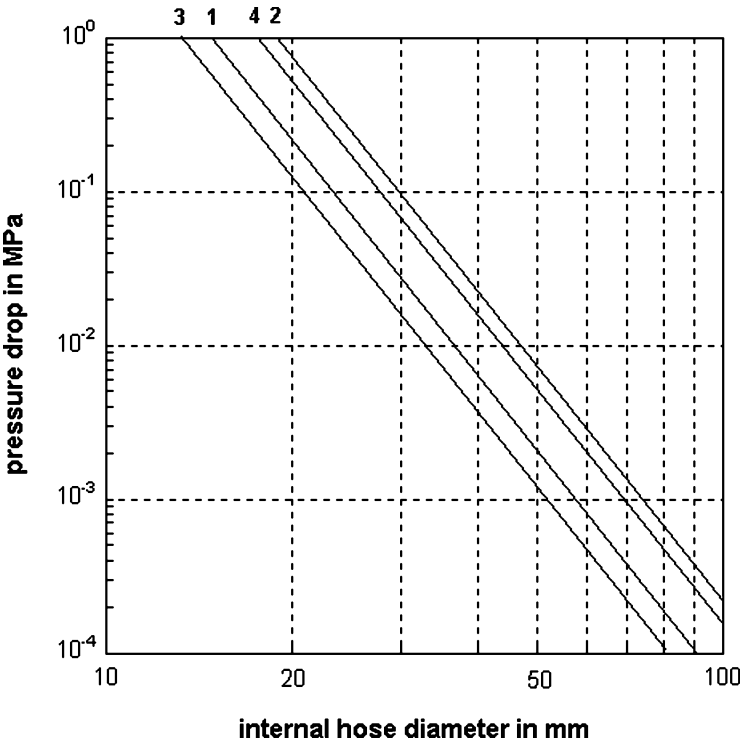

Fig. 4.24 Results of (4.14); hose length: $l_H = 40\,m$. Conditions: "1" – $p = 0.7\,MPa$, $\dot{Q}_A = 5.0\,m^3/min$; "2" – $p = 0.7\,MPa$, $\dot{Q}_A = 10\,m^3/min$; "3" – $p = 1.0\,MPa$, $\dot{Q}_A = 5.0\,m^3/min$; "4" – $p = 1.0\,MPa$, $\dot{Q}_A = 10\,m^3/min$

Another principle for the assessment of pressure drops in armatures is the *equivalent length*. It is assumed that the pressure drop in a certain type of armature corresponds to the pressure drop in a pipe of a certain *equivalent length*. Examples for this procedure are provided in Table 4.8. If, for example, a seat valve with an inlet pipe diameter of 40 mm is considered, the equivalent length is 10 m. These two values must now be inserted into (4.14) in order to calculate the approximate pressure drop for this particular armature ($d_H = 40\,mm$, $l_H = 10\,m$). More examples can be found in Bohl (1989).

4.5 Abrasive Hose Lines

4.5.1 Conveying Modes in Abrasive Hoses

Abrasive hoses serve to convey the abrasive materials from the blast machine to the blast cleaning nozzle. This process can be considered pneumatic conveying, and

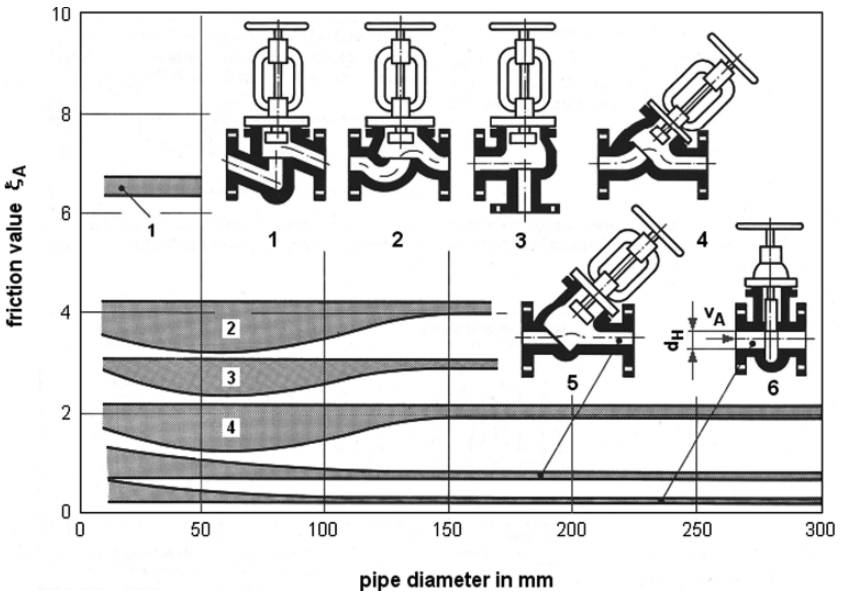

Fig. 4.25 Typical friction values for valve armatures (Wagner, 1990)

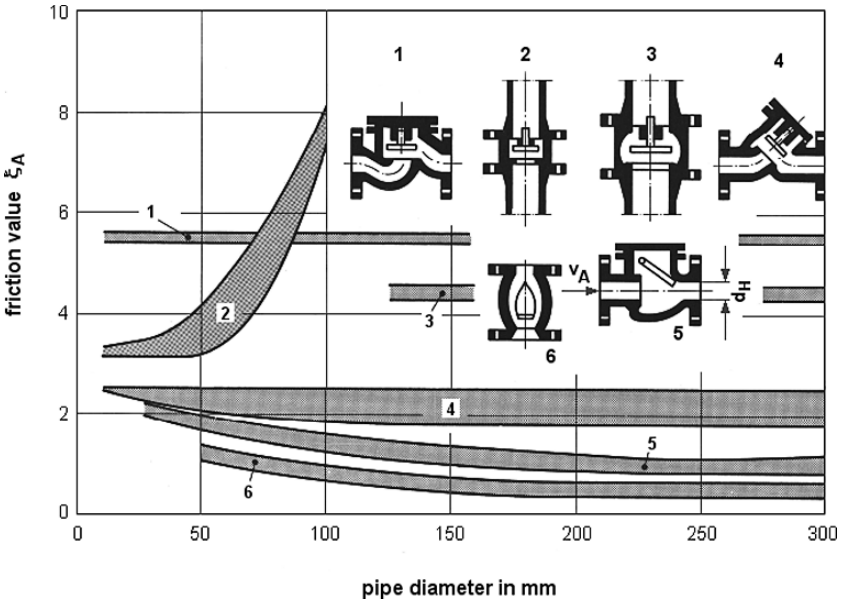

Fig. 4.26 Typical friction values for check valves (Wagner, 1990)

Table 4.8 *Equivalent lengths* for numerous air armatures (Fraenkel, 1954)

Armature	Equivalent length in m						
	Pipe diameter in mm						
	25	40	50	80	100	125	150
Seat valve	6	10	15	25	30	50	60
Streamline valve	3	5	7	10	15	20	25
Gate valve	0.3	0.5	0.7	1	1.5	2	2.5
Bend (peak corner)	1.5	2.5	3.5	5	7	10	15
Bend (smooth corner)	1	2	2.5	4	6	7.5	10
Bend ($r = D$)	0.3	0.5	0.6	1	1.5	2	2.5
Bend ($r = 2D$)	0.15	0.25	0.3	0.5	0.8	1	1.5
Hose coupling (T-shape)	2	3	4	7	10	15	20
Reducer	0.5	0.7	1	2	2.5	3.5	4

relationships known from pneumatic conveying techniques can, to a certain amount, be utilised.

Engineering treatments on pneumatic conveying processes can be found in Buhrke et al. (1989), Marcus et al. (1990), Siegel (1991) and Weber (1974). For fine particles suspended in an air stream, two basic conveying modes can occur: stable flow and unstable flow. Moreover, five different flow patterns can be observed, namely fully suspended (stable), surging (unstable), stationary bed (stable), moving bed (very unstable) and stationary bed (stable). These patterns depend on air conveying velocity and abrasive mass flow rate. Some relationships are illustrated in Figs. 4.27–4.29. Stable conveying conditions are one preposition for an efficient functioning of abrasive hose systems. The graphs plotted in Fig. 4.28 show, in particular, how changes in air flow velocity and abrasive mass flow rate affect the flow regime. An air flow velocity of $v_F = 15$ m/s and an abrasive mass flow rate of $\dot{m}_P = 4$ t/h (67 kg/min) lead to "instable region" flow. If the air flow velocity is increased up to $v_F = 20$ m/s, the process turns into a more effective "hank conveying", whereby the pressure drop slightly increases. "Hunk conveying" can also be obtained, if the abrasive mass flow rate is reduced to $\dot{m}_P = 2$ t/h (33 kg/min). For this condition, the flow turns into "hank conveying", whereby the original air flow velocity ($v_F = 15$ m/s) can be maintained.

4.5.2 Critical Conveying Flow Velocities in Abrasive Hoses

The graphs plotted in Figs. 4.27–4.29 show that a typical air flow velocity exists where pressure drop has minimum values. This flow velocity is denoted "critical air velocity" in Fig. 4.27. The higher the abrasive mass flow rate, the higher is the value for this optimum air flow velocity. This trend is illustrated in Fig. 4.29 by the line designated "optimum". For a typical blast cleaning condition (e.g. $\dot{m}_P = 16$ kg/min), the optimum air flow velocity may be in the range of $v_F = 16$ m/s. If the abrasive mass flow rate is reduced to $\dot{m}_P = 4.2$ kg/min, the optimum flow velocity is about $v_F = 12$ m/s (see Fig. 4.29).

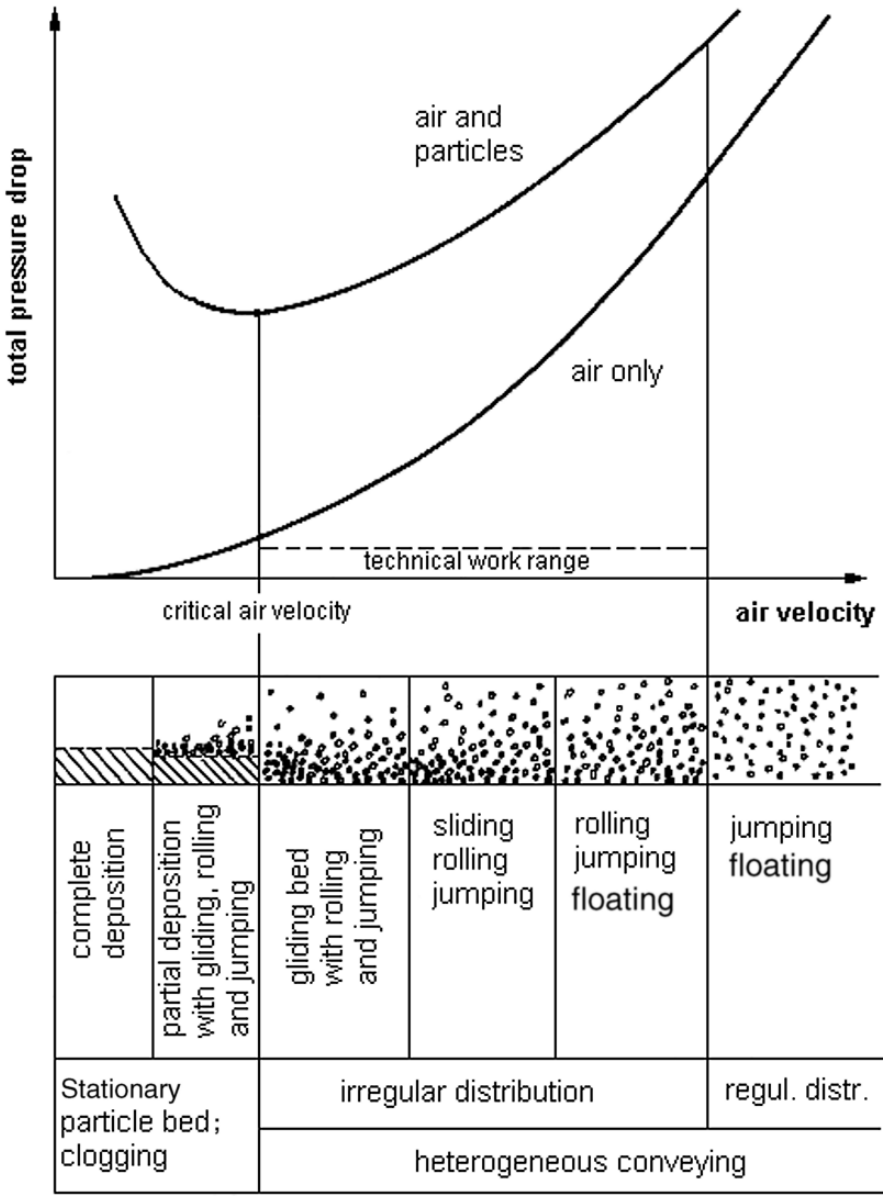

Fig. 4.27 Conveying modes in pneumatic solid particle conveying lines: general relationships (Buhrke et al., 1989)

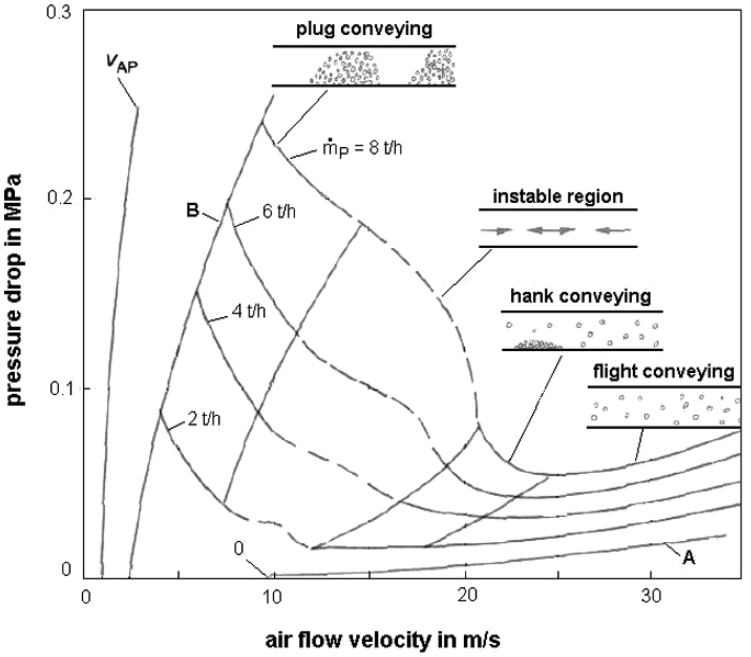

Fig. 4.28 Effect of abrasive mass flow rate on conveying modes in pneumatic solid particle conveying lines (Siegel, 1991); see text for the meanings of "A" and "B"

The line "A" in Fig. 4.28 characterises the plain air flow without any solid particles. The relationship is $\Delta p_A \propto v_F^2$. The line "B" in Fig. 4.28 marks the limits for abrasive conveying for a given abrasive mass flow rate. For $\dot{m}_P = 4$ t/h (67 kg/min), the limiting flow velocity is at about $v_F = 7$ m/s. But the conveying process is still possible for the lower mass flow rate ($\dot{m}_P = 2$ t/h).

The line "v_{AP}" in Fig. 4.28 characterises the general limit for any pneumatic conveying for the given solid material. This critical velocity, called "saltation velocity", is about $v_{AP} = 3$ m/s for the conditions in Fig. 4.28. Each abrasive material requires a saltation velocity, which is the minimum gas flow velocity for horizontal conveying. Certain approaches are known for the analytical estimation of this parameter. A rather simple approach is due to Rizk (1973):

$$\frac{\dot{m}_P}{\dot{m}_A} = \frac{1}{10^{1.44 \cdot d_P + 1.96}} \cdot \left[\frac{v_{AP}}{(g \cdot d_H)^{1/2}} \right]^{1.1 \cdot d_P + 2.5} \tag{4.24}$$

It can be seen from (4.24) that the saltation velocity depends on the mass flow ratio abrasive/air, hose diameter (m) and abrasive particle size (mm). Uferer (1992) adapted a similar model for the use in blast cleaning hoses, and he derived the following relationship:

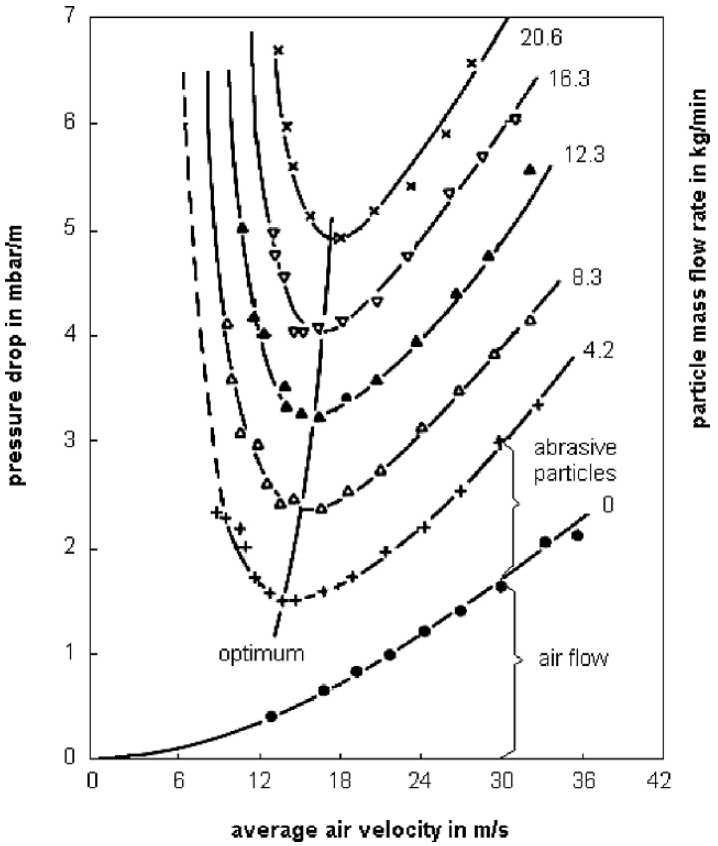

Fig. 4.29 Relationships between air velocity, abrasive mass flow rate, and pressure loss in pneumatic conveying lines (Marcus et al., 1990)

$$v_{AP} = 18.8 \cdot \left(\frac{\dot{m}_P}{\dot{m}_A}\right)^{1/3} \cdot d_H^{1/2} \cdot g^{1/2} \tag{4.25}$$

In this simplified approach, abrasive particle size is excluded. For typical conditions ($\dot{m}_P/\dot{m}_A = 1.5$, $d_H = 35$ mm), the critical air conveying velocity is about $v_{AP} = 13$ m/s. Further results are plotted in Fig. 4.30. It can be seen that saltation velocities typically between $v_{AP} = 10$ m/s and 15 m/s are required for blast cleaning applications.

The actual demanded air velocity in an abrasive hose can be adjusted through variations in the ratio between abrasive hose diameter and nozzle diameter according to the following approach suggested by Uferer (1992):

$$\left(\frac{d_H}{d_N}\right)^2 = \frac{181}{v_F} \tag{4.26a}$$

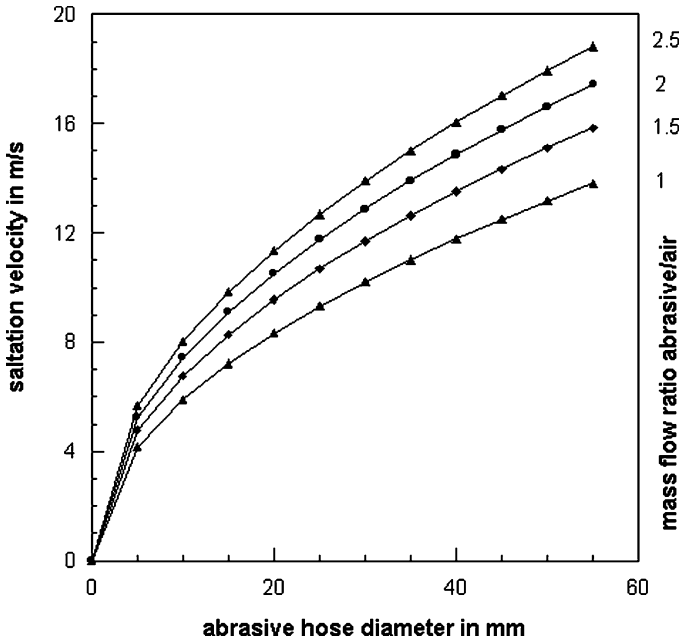

Fig. 4.30 Saltation air flow velocity for particle conveying, based on (4.25)

This relationship holds if air temperature does not vary, and if the air pressure exceeds the value of $p = 0.09$ MPa. Results of calculations are plotted in Fig. 4.31. If a value of $v_F = 15$ m/s for the air velocity is being considered (which is just above the saltation velocity), an optimum diameter ratio is at about $d_H/d_N = 3.5$. This result agrees well with recommendations issued by equipment manufacturers, and it verifies the application of methods developed for pneumatic conveying of solids to the condition in blast cleaning hoses. If, for example, a nozzle with a diameter of $d_N = 12$ mm and a mass flow ratio abrasive/air of $R_m = 1.5$ are used, the optimum abrasive hose diameter would be $d_H = 42$ mm according to (4.26a). The next larger standard hose diameter is $d_H = 50$ mm, which would deliver a diameter ratio of 50/12 = 4.2. From (4.26a), the corresponding air flow velocity is about $v_F = 10$ m/s, which is lower than the typical saltation velocity plotted in Fig. 4.30 for $d_H = 50$ mm (which is $v_{AP} = 15$ m/s). Thus, unsteady abrasive conveying, or even clogging, may occur, which would increase pressure losses in the hose because of air flow through deposited abrasive particle conglomerates (this would apply to the region left from the line marked by "critical air velocity" in Fig. 4.27). The next smaller standard hose diameter is $d_H = 38$ mm, which leads to an increase in air flow velocity up to $v_F = 18$ m/s. Although the flow is now in the "technical working range" (see Fig. 4.27), this rather high flow velocity would notably increase pressure drop (compare also Fig. 4.29). Equation 4.26a is valid in that particular configuration only for $l_H = 0$ (pressure drop in hoses is not considered). For the case $l_H > 0$, the relationship must be modified as follows (Uferer, 1992):

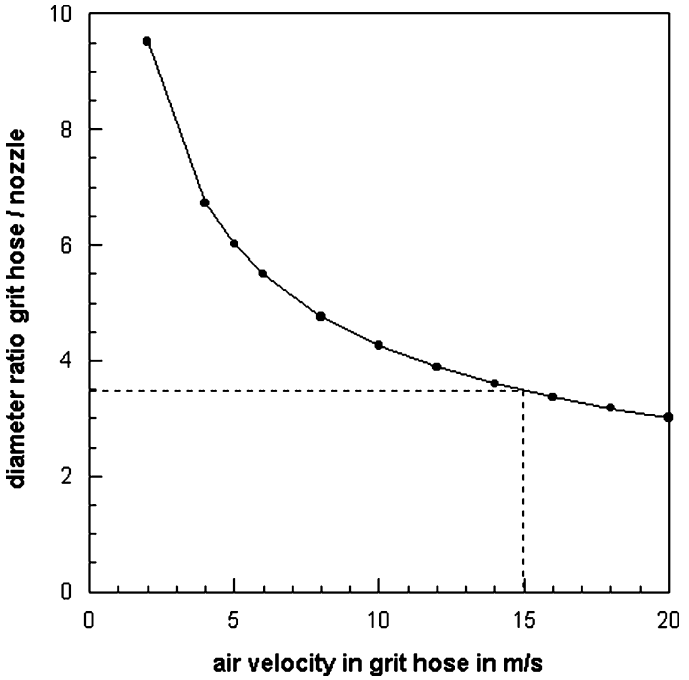

Fig. 4.31 Relationships between air velocity, abrasive hose diameter and nozzle diameter, based on (4.26a)

$$\left(\frac{\mathrm{d_H}}{\mathrm{d_N}}\right)^2 = \frac{181}{\mathrm{v_F}} \cdot \left(\frac{1}{1 + (\Delta \mathrm{p_T}/\mathrm{p})}\right) \tag{4.26b}$$

For $\Delta p_T = 0$, (4.26b) reduces to (4.26a). For an assumed pressure drop of 25% and an air flow velocity $v_F = 15$ m/s, (4.26b) delivers an optimum ratio $d_H/d_N = 3.1$. For the example mentioned earlier ($d_N = 12$ mm), the optimum hose diameter is $d_H = 37.2$ mm. The next commercially available hose diameter is $d_H = 38$ mm, which is very close to the requested value. Because the pressure drop is a function of the hose length, the diameter ratio d_H/d_N depends on hose length. In an optimum blast cleaning system, the parameters d_N, d_H and l_H are well balanced, and if one of the parameters changes value, the other parameters must be adjusted accordingly.

4.5.3 Optimum Flow Velocities in Abrasive Hoses

Pressure drop in abrasive hose lines is due to air flow and abrasive material conveying in these hoses. Experience with pneumatic conveying systems has shown that pressure drop depended on air conveying velocity (respectively, dynamic air pressure and air flow Froude number) and mass flow ratio abrasive/air. One example is shown in Fig. 4.29; more information can be found, among others, in Coulson and

Richardson (1968) and Marcus et al. (1990). It can be recognised from the graph in Fig. 4.29 (as well as from Figs. 4.27 and 4.28) that the pressure drop for a solid-air flow is much higher compared with that for a plain air flow. For an air conveying velocity $v_F = 15$ m/s, the pressure drop is $\Delta p_T = 0.5$ mbar/m for air only, but it is about $\Delta p_T = 2.4$ mbar/m for $\dot{m}_P = 8.3$ kg/min. It can also be noted from Fig. 4.29, that pressure loss has distinct minimum values at certain optimum air conveying velocities. This optimum air flow velocity depends on the Froude number of the particle settling flow. For vertical conveying processes, the optimum air flow velocity can be approximated as follows (Ahland, 1966):

$$v_{opt} = 4.1 \cdot g^{0.2} \cdot d_H^{0.2} \cdot v_S^{0.6} \tag{4.27}$$

This equation is valid for a range of Froude numbers (related to settling speed) between $Fr = 2.5$ and 25. The relationship is graphically expressed in Fig. 4.32 for typical blast cleaning conditions. It is important to note that the optimum air conveying velocity depends on hose diameter, although hose size effects become considerable in the range of rather high settling velocities. The settling velocities of abrasive particles in air must be estimated experimentally. Weber (1974) published an extensive number of experimental results. If particle material density and

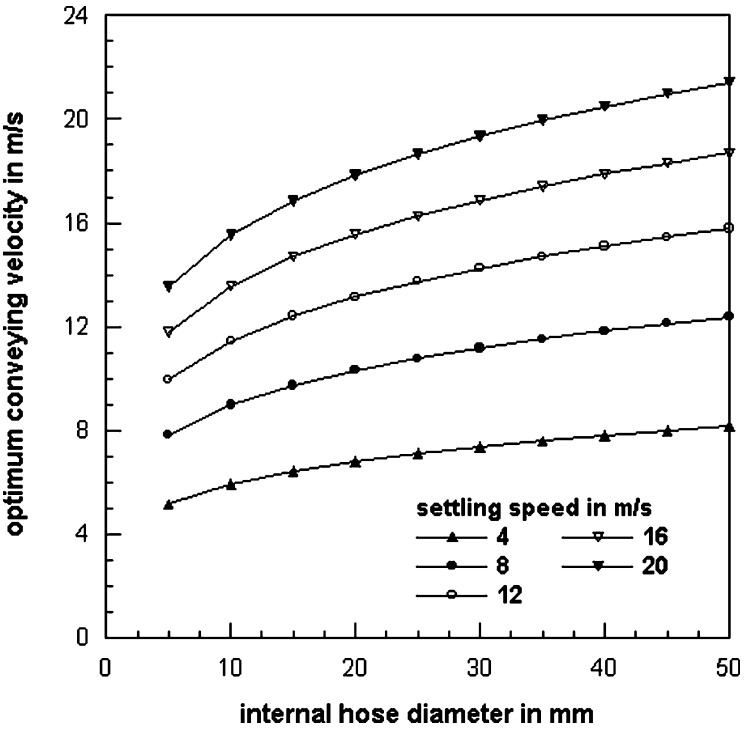

Fig. 4.32 Optimum air velocity for vertical conveying according to (4.26)

particle diameter are known, the settling velocity in air can be read from the corresponding graphs. If only particle properties are considered, and gas properties (mainly density) are excluded, settling velocity drops if particle size and particle material density decrease. A copper slag particle ($\rho_P = 3{,}700\,kg/m^3$) with a size of $d_P = 1{,}000\,\mu m$ has a settling speed of about $v_S = 9\,m/s$, whereas a steel shot particle ($\rho_P = 7{,}000\,kg/m^3$) of equal size has a settling velocity of about $v_S = 15\,m/s$. The graphs in Weber's (1974) book are restricted to spherical particles, but a comparison with results of other authors supports the suitability for other particle shapes. Buhrke et al. (1989) published correction factors, which consider effects of particle shape, turbulence degree and particle interactions. More importantly, the graphs plotted in Weber's (1974) book do not consider effects of air density; they apply to atmospheric conditions only, and they may deliver different results if air density variations due to higher air pressures in the hose are taken into account. Some limited measurements of settling velocities of particles in air under different air pressures are reported by Seville et al. (1997). Some of their results are plotted in Fig. 4.33. It can be seen that the air pressure notably affects the settling velocity. For the particles with a diameter of $d_P = 1{,}000\,\mu m$ suspended in an air temperature of $\vartheta = 27°C$ ($T = 300\,K$), the settling velocity is $v_S = 7\,m/s$ for an air pressure of $p = 0.1\,MPa$, but it is $v_S = 2.5\,m/s$ only for an air pressure of $p = 1.0\,MPa$. This is a reduction of –64%. The effects of air pressure are more pronounced for the larger particle size. A typical average reduction value would be about -50% for the conditions considered in Fig. 4.33. If this reduction factor is applied to (4.27), it can be seen that the optimum air flow velocity changes by a factor of $0.5^{0.6} = 0.66$.

4.5.4 Pressure Drop in Abrasive Hoses

A general formal approach for estimating the pressure drop in an abrasive hose line is as follows:

$$\Delta p_T = \Delta p_A + \Delta p_P \tag{4.28}$$

Here, Δp_A is the pressure drop due to air flow, and Δp_P is the pressure drop caused by abrasive conveying. This relationship is illustrated in Fig. 4.29. In the figure, the lowest line (denoted "0") illustrates the pressure drop due to plain air flow, whereas the next line (denoted "4.2") characterises the total pressure drop due to air flow and abrasive conveying (in that particular case for $\dot{m}_P = 4.2\,kg/min$). The vertical distance between these two lines, designated "abrasive particles", characterises the pressure drop caused by the abrasive conveying process. The additional pressure loss Δp_P is for two reasons. First, the settling movement of the solid particles in the hose must be balanced; second, the solid particles affect the conditions of the air flow. Based on (4.13) and (4.14), a suitable approach is as follows:

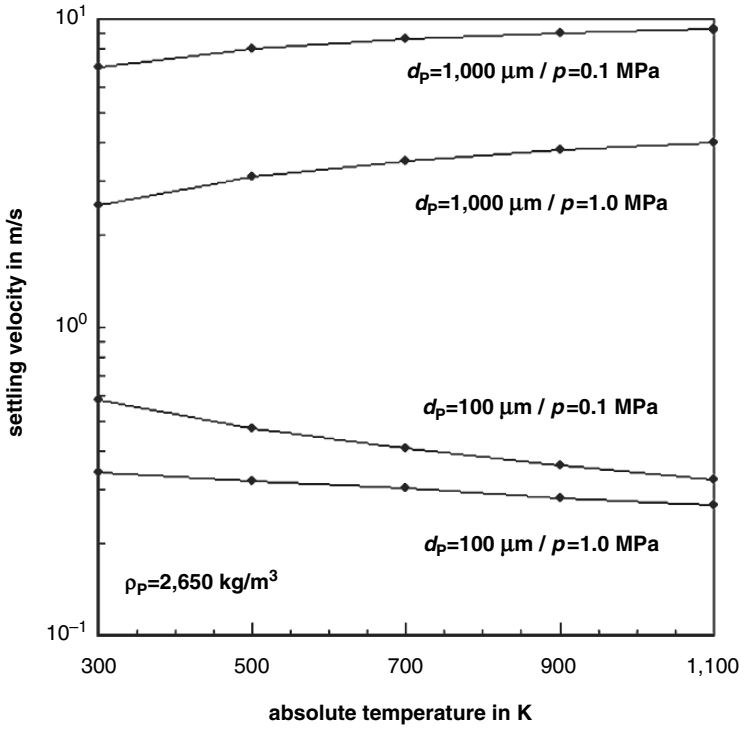

Fig. 4.33 Relationship between air density, particle size and settling velocities for grit particles in air (Seville et al., 1997)

$$\frac{\Delta p_T}{\rho_A} = \underbrace{(\lambda_A + \lambda_P) \cdot \frac{l_H}{d_H} \cdot \frac{v_F^2}{2}}_{\text{straight hose}} + \underbrace{(\xi_A + \xi_P) \cdot \frac{v_F^2}{2}}_{\text{knee or armature}} \tag{4.29}$$

The parameters λ and ξ are friction numbers. The subscript "A" stands for air flow, whereas the subscript "P" stands for abrasive conveying. The friction parameter λ_A can be calculated with (4.21). Corresponding values can be found in Fig. 4.21. The parameter λ_P can be approximated with pneumatic conveying arguments. An approach delivered by Uferer (1992) is as follows:

$$\lambda_P = \frac{C_P}{Fr_P^{\alpha_F}} \tag{4.30}$$

The constant C_P as well as the power exponent α_F depend on abrasive properties. The Froude number is given as follows:

$$Fr_P = \frac{v_F}{(d_P \cdot g)^{1/2}} \tag{4.31}$$

Uferer (1992) performed a number of experiments in order to specify (4.30) for the conditions in blast cleaning hoses. He derived the following semi-empirical relationship:

$$\lambda_P = \frac{C_{TP}}{Fr_P^{0.15}} \cdot \left(\frac{\dot{m}_P}{\dot{m}_A}\right)^{1.8} \tag{4.32}$$

The approach is valid for Froude numbers between $Fr_P = 30$ and 200, and for mass flow ratios abrasive/air between $R_m = 0.5$ and 5.0. The constant C_{TP} is an abrasive material parameter. Typical values for this parameter are listed in Table 4.9. A very rough approximation for slag materials and quartz is as follows (Uferer, 1992):

$$C_{TP} = 0.014 \cdot v_S \tag{4.33}$$

The graphs in Fig. 4.33 can be utilised for the approximation of v_S-values. If an average value of $v_S = 5$ m/s is taken from Fig. 4.33 for $d_P = 1{,}000$ μm in the pressure range between $p = 0.1$ MPa and 1.0 MPa, (4.33) delivers $C_{TP} = 0.07$. This value is in the range for quartz sand and lead-thin slag (see Table 4.9). Results of measurements are compared with results based on (4.32) in Fig. 4.34. Typical values are between $\lambda_P = 0.05$ and 0.2. In certain cases, these values are one order of magnitude larger than friction values for the flow of air only (see Fig. 4.21 for comparative values). This is shown by the dotted line in the lower section of the graph, which characterises a typical friction parameter for the air flow under the given conditions. The lines "1" to "4" in Fig. 4.34 refer to results obtained with the calculation model discussed earlier for two abrasive materials and for different mass flow ratios abrasive/air. These lines follow the relationship $\lambda_P \propto Fr_P^{-0.15}$. The lines "1" (nickel slag, $R_m = 2.0$) and "4" (quartz sand, $R_m = 1.0$) mark typical upper and lower limits for the friction numbers in abrasive hoses. Equations (4.30)–(4.33) can be applied to approximate values for λ_P under different process conditions.

The values for λ_P in Fig. 4.34 are notably higher than values for friction numbers for pneumatic conveying in rigid pipes. Typical examples for friction values for pneumatic conveying in rigid pipes are listed in Table 4.10. More examples are published in Marcus et al. (1990). The reasons for the higher values for the blast cleaning process are that flexible rubber hoses are used for blast cleaning, and that the abrasive particles act as erosive media. Results listed in Table 4.10 very effectively illustrate the effect of material parameters on the friction number. If the hardness of the pipe material drops, friction value increases by a factor of 5

Table 4.9 C_{TP}-values for some abrasive materials (Uferer, 1992)

Abrasive material	C_{TP}-value
Lead–tin slag	0.078
Phosphor slag	0.102
Iron–nickel slag	0.129
Quartz sand	0.07

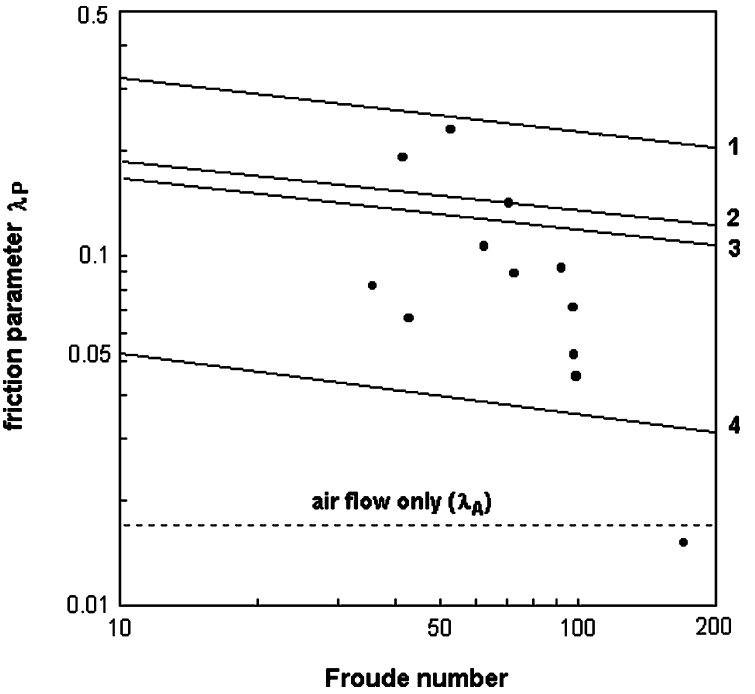

Fig. 4.34 Relationship between Froude number and friction parameter for abrasive-air flow in abrasive hoses (based on results reported by Uferer, 1992). 1 – nickel slag ($R_m = 2.0$); 2 – nickel slag ($R_m = 1.5$); 3 – quartz sand ($R_m = 2.0$); 4 – quartz sand ($R_m = 1.0$)

for quartz. If the abrasive particle material hardness increases (from Mohs 5.5 for glass beads to Mohs 7 for quartz), friction value also increases notably. This latter effect very well demonstrates that hose (with respect to pipe) material erosion has a notable influence on the friction number.

A plainly empirical approach is due to Gasterstädt (1924), who found the following relationship for pressure losses in conveying pipes based on extensive experimental work:

Table 4.10 Effects of material properties on the friction factor in rigid pipes (Weber, 1974)

Abrasive material	Pipe material	Friction factor λ_P	
		Absolute	Relative
Glass beads ($d_P = 4.0$ mm)	Steel (hardened)	0.0025	1.00
	Steel (not hardened)	0.0032	1.28
	Aluminium	0.0051	2.04
	Copper	0.0053	2.12
Quartz ($d_p = 3.0$–5.0 mm)	Steel (hardened)	0.0060	2.40
	Steel (not hardened)	0.0072	2.88
	Aluminium	0.0184	7.36
	Copper	0.0310	12.40

$$\frac{\Delta p_T}{\Delta p_A} = 1 + C_\lambda \cdot \frac{\dot{m}_P}{\dot{m}_A} \tag{4.34}$$

For the case $\dot{m}_P/\dot{m}_A = 0$, (4.34) delivers $\Delta p_T = \Delta p_A$. The empirical constant C_λ characterises the effects of abrasive and pipe wall material; it takes typical values for certain material combinations. Values for this parameter must be estimated by experiments. It can be concluded from the discussion in the previous section that C_λ has high values for hard, irregularly shaped solid particles. An exploitation of experimental results reported by Uferer (1992) for mass flow ratios abrasive/air between $R_m = 1.0$ and 2.0 delivers typical values of $C_\lambda = 1$–4 for slag materials as well as for quartz sand conveyed in blast cleaning hoses. An analysis of the reported results depicted that the C_λ-values showed a relationship to the hose diameter. The larger the hose diameter, the higher were the values for C_λ. Equation (4.34) is graphically expressed in Fig. 4.35 for different C_λ-values. It can be seen that the pressure drop ratio can become as high as $\Delta p_T/\Delta p_A = 10$ for typical mass flow ratios abrasive/air. Although Gasterstädt's (1924) relation helps to find pressure loss values from a restricted number of measurement, its physical relevance is controversial. This approach cannot be used for the estimation of the individual pressure drop caused by abrasive addition. Another critical issue is that $\dot{m}_p$ and $\dot{m}_A$ cannot be varied independently on each other if nozzle flow is considered.

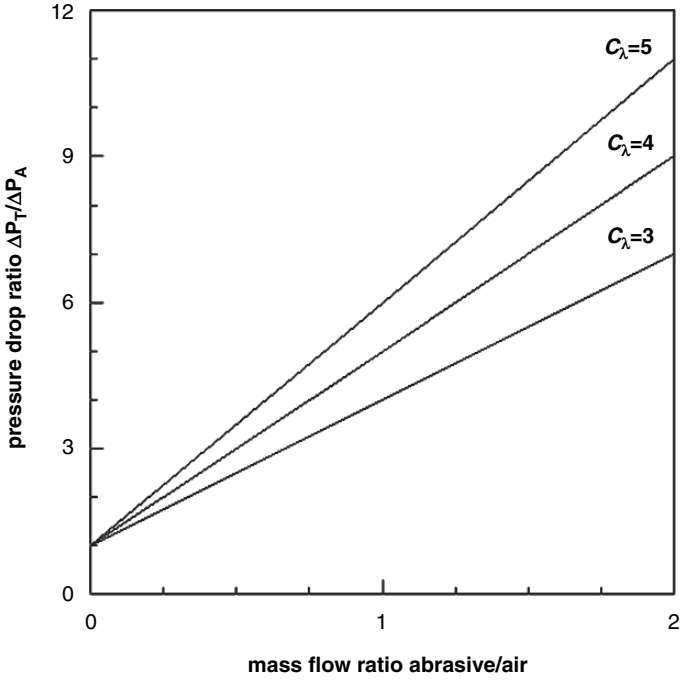

Fig. 4.35 Graphical expression of Gasterstädt's relation for different C_λ-values

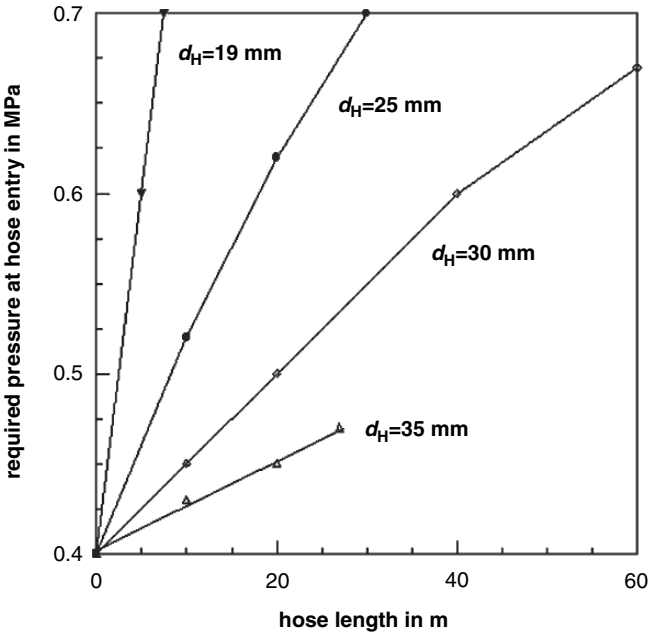

Fig. 4.36 Experimentally estimated pressure drop values in abrasive hoses (Uferer, 1992)

Uferer (1992) performed systematic measurements of pressure drops in blast cleaning abrasive hoses. Results of his work are provided in Fig. 4.36. The graphs not only illuminate the dominating effect of the hose diameter, but also verify that pressure loss is more severe in abrasive hose lines compared with plain air hose lines (compare Fig. 4.24). If a hose with a diameter of $d_H = 25$ mm is in operation, the pressure drop reaches a value of $\Delta p_T = 0.45$ MPa after a distance of $l_H = 3$ m. If the operator can choose either a long air hose line or a long abrasive hose to be utilised, abrasive hose line must be as short as possible.

Results of numerical simulations performed by Tashiro and Tomita (2004) for the calculation of pressure drops in pipes for horizontal pneumatic transport depicted notable effects of abrasive material density, air flow velocity and mass flow ratio abrasive/air on the additional pressure drop caused due to abrasive addition. The additional pressure drop caused by the addition of abrasive particle to the air flow was very pronounced for abrasive materials with rather low densities. If particles with a density of $\rho_P = 2{,}000\,\text{kg/m}^3$ were added into an air stream with a flow velocity of about $v_F = 28$ m/s, the additional pressure drop was about $\Delta p_P = 50$ Pa/m for a mass flow ratio of $R_m = 2$. If particles with a density of $\rho_P = 1{,}000\,\text{kg/m}^3$ were added, the additional pressure drop increased to a value as high as $\Delta p_P = 200$ Pa/m. If the air flow velocity was reduced down to $v_F = 19$ m/s, the values for the additional pressure drop were reduced down to $\Delta p_P = 7$ Pa/m ($\rho_P = 2{,}000\,\text{kg/m}^3$, $R_m = 2$),

respectively to $\Delta p_P = 25$ Pa/m ($\rho_P = 1{,}000\,kg/m^3$, $R_m = 2$). Distinguished effects of air compressibility on the additional pressure drop could not be estimated by Tashiro and Tomita (2004).

Results of measurements on pressure drop in grit hose performed by Bae et al. (2007) were already shown in Fig. 4.13. The lines illustrate the effects of abrasive mass flow rate and nozzle design on the pressure drop. The curves can be fitted with a simple linear law according to the following equation:

$$\Delta p_T = C_1 \cdot \dot{m}_P + C_2 \tag{4.35}$$

The pressure drop is given in MPa, and the abrasive mass flow rate in given in kg/min. The precise values for the regression parameters C_1 and C_2 depend on the geometry of the nozzle. The regression is valid for rather high abrasive mass flow rates between $\dot{m}_P = 11$ kg/min and 40 kg/min. It can only be applied to determine trends, because the hose length was not given in Bae et al. (2007) work. Comparative pressure drop measurements were performed by Bosshard and Fritchman (1992). The authors used steel shot (S110) and deployed moderate air pressures ($p = 0.12$–0.45 MPa) and moderate abrasive mass flow rates ($\dot{m}_P = 0.8$–5.0 kg/min). The ratio between hose diameter and nozzle diameter was $d_H/d_N = 2.5$. The authors found that the pressure drop in abrasive hoses increased linearly with an increase in abrasive mass flow rate. The pressure drop ratio between plain air flow ($\dot{m}_P = 0$) and flow with abrasive material was between $\Delta p_P/\Delta p_A = 1.5$ to 3, and this ratio depended on the abrasive mass flow rate.

The graphs presented in Figs. 4.13 and 4.36 demonstrate that the working line of a nozzle, as plotted in Fig. 4.3, is a function of the pressure drop in the blast cleaning system. An ideally performing system would permanently cross-check the actual nozzle working line with the compressor working line, and it would take corrective action.

Figure 4.37 illustrates the effect of the abrasive hose dimensions on the relative cleaning rate. The graphs are based on measurements performed by Uferer (1992). If pressure drop is not considered ($l_H = 0$), the systems with the nozzle diameter $d_N = 8$ perform at a relative cleaning rate of 100%. If the nozzle diameter increases up to $d_N = 10$ mm (e.g. due to nozzle wear), and no buffer vessel is placed between compressor and nozzle, the efficiency notably drops down to 64%. However, the situation changes if abrasive hoses are considered. It can be seen that the efficiency notably drops for the system with the smaller hose diameter ($d_H = 25$ mm). This effect is due to the severe pressure drop in the narrow hose. If a hose length as short as $l_H = 20$ m is exceeded, this system performs worse than the system with the larger nozzle diameter. At a hose length of $l_H = 50$ m, this system delivers only 40% of the original cleaning rate. For very long hoses ($l_H > 70$ m), the two systems with the larger hose diameter ($d_H = 32$ mm) perform almost equally good. This discussion very well illustrates the complex relationships behind any blast cleaning optimisation procedure.

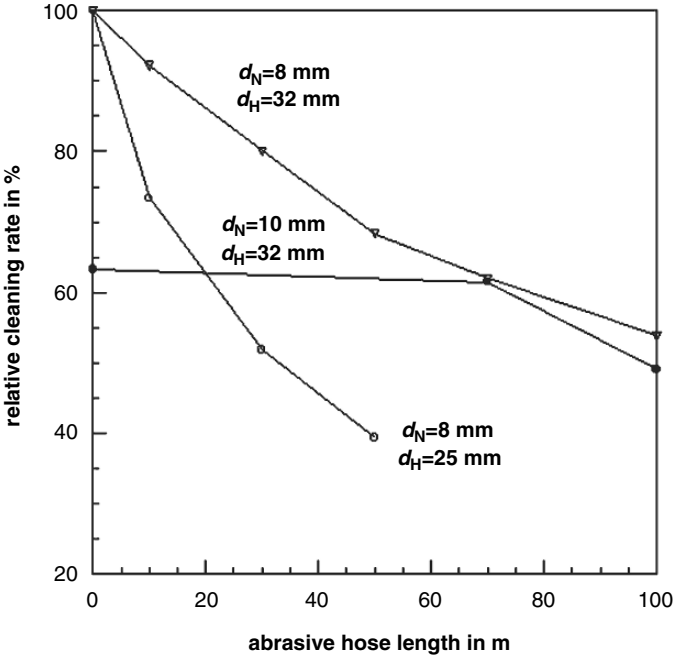

Fig. 4.37 Relationship between nozzle diameter, abrasive hose diameter, abrasive hose length and relative cleaning rate (based on measurements reported by Uferer, 1992)

4.6 Nozzles

4.6.1 Nozzle Types

For blast cleaning operations, the following two prime nozzle types can be distinguished:

- cylindrical nozzles with convergent inlet sections;
- nozzles with a convergent–divergent shape (Laval nozzles).

The performance characteristics of both nozzle types are described in Chap. 3.

For convergent–divergent nozzles, Settles and Geppert (1997) issued the following optimisation design rules:

- The convergent section should be minimised to bring the Mach number between air and abrasive particles to unity ($Ma = 1$) as soon as possible.
- The throat section should not be longer than necessary to avoid its wearing.
- The divergent nozzle section should be contoured rapidly until the Mach number between air and abrasive particles reaches a value of about $Ma = 1.4$ (see Fig. 3.18).
- The divergent contouring should be gradually maintained to maintain the relative Mach number of $Ma = 1.4$.

- The length of the divergent section should be extended as required to achieve the desired abrasive particle velocity at the nozzle exit.
- The ratio between nozzle exit area and nozzle throat area should be chosen for the given exit pressure to be near perfect expansion (see Fig. 3.24).

Each individual blast cleaning nozzle has its particular working line, which is given as follows:

$$\mathrm{p} = f(d_\mathrm{N}) \cdot \dot{\mathrm{Q}}_\mathrm{A} \tag{4.36}$$

Three examples for nozzle working lines are plotted in Fig. 4.3. The functions depict a linear relationship between the two parameters (see Sect. 3.2.1). The fundamentals of nozzle flow are discussed in Sect. 3.2.

Blast cleaning nozzles consist of a nozzle body (housing) and an inlet section. Whereas the body is usually made from steel, the inlet sections are made from different materials, including steels, tungsten carbides, ceramics and composite materials.

4.6.2 Nozzle Wear

4.6.2.1 Fundamentals of Nozzle Wear

Nozzle wear is a serious problem with any blast cleaning system. Nozzle wear deteriorates efficiency and often avoids a continuous blast cleaning operation. The basic mechanism is the erosion of the nozzle wall due to impinging abrasive particles. The processes discussed in Chaps. 2 and 5 relate on nozzle wear as well.

Ishii and Kawasaki (1982) performed numerical simulations of the particle streamlines in blast cleaning nozzles. Their results deduced an upper limiting point in the wall region where the particle could impinge, when the impingement of the particles on the nozzle wall occurred in the supersonic section of the nozzle (see Sect. 3.3). The location of this point did not depend on particle size, but on nozzle geometry.

Examples of worn blast cleaning nozzle inlet sections are shown in Fig. 4.38. The images “a” and “c” illustrate the wear of an aluminium oxide nozzle, whereas the images “b” and “d” illustrate the wear of a boron carbide nozzle. It can be seen that the wear did not occur regularly, but rather concentrated in the upper section of the nozzle inlet. Figure 4.39 provides information on the change in the internal nozzle geometry due to wear. It can be seen that the erosion was not regular over the nozzle length; the worn cross-section rather moved towards the nozzle exit over time. But the minimum cross-section, which determines air flow rate and air flow velocity (see Sect. 3.2), was already extended after 6 hours. After an exposure time of $t_\mathrm{B} = 20\,\mathrm{h}$, this worn section had reached the nozzle exit. Similar observations were reported by Lukschandel (1973). Observations have shown that the internal geometry of cylindrical nozzles without a convergent inlet section changed over the time; their geometry approached that of convergent–divergent (Laval) nozzle. The same happened with cylindrical nozzles that already contained a convergent

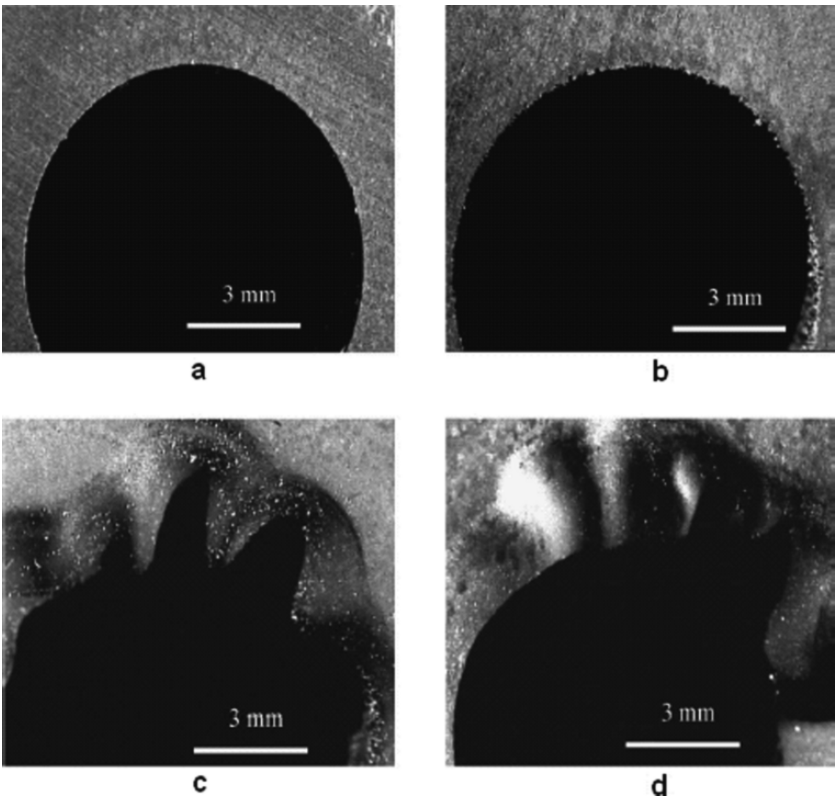

Fig. 4.38 Entry sections of ceramic blast cleaning nozzles (Deng et al., 2003b). (**a**) New aluminium oxide nozzle; (**b**) New boron carbide nozzle; (**c**) Worn aluminium oxide nozzle after $t_B = 4\,h$; (**d**) worn boron carbide nozzle after $t_B = 4\,h$

inlet section (Pashatskii et al., 1971; Kumar et al. 1983). An example is provided in Fig. 4.40. The dotted line expresses the shape of the worn steel nozzle after an operation period of 25 min. It seemed that the wear, in terms of diameter, increased to approach a saturation value for a given ratio between (eroded) exit diameter and bore diameter; values for this ratio were reported to be between 3 and 5 for conical nozzles (Pashatskii et al. 1971). Sheldon et al. (1977) sectioned an aluminium tube ($d_N = 5\,mm$, $l_N = 305\,cm$) into individual short tube sections 2.54-cm long. Each individual tube section was carefully weighed, and the tube sections were then re-assembled to form a tube of original length. This tube was eroded with hardened steel shot ($d_P = 270\,\mu m$; $\dot{m}_P = 1.26\,g/s$, $p = 0.17\,MPa$). After eroding, the tube was disassembled and each section was weighed. It was noted that the erosion rate (kg/kg) was very low at the inlet section of the tube, where the velocity of the particles was rather low, and then rose in a non-linear manner to a maximum value at the exit section of the tube. Deng (2005b) scanned the internal profile of a ceramic nozzle eroded over a period of 50 hours. Results of this study are displayed

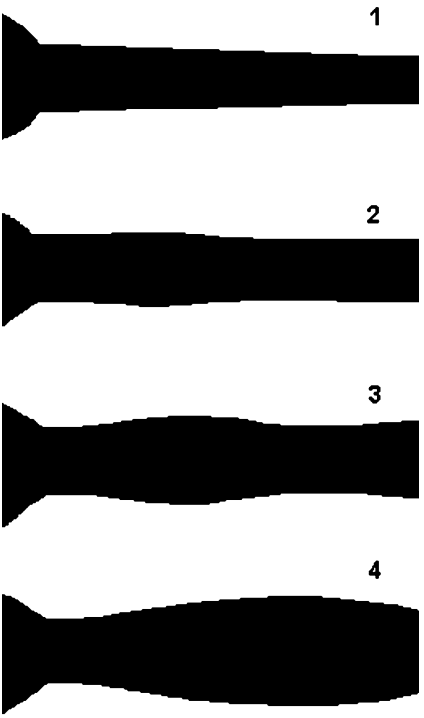

Fig. 4.39 Wear pattern in a blast cleaning nozzle (Gesell, 1969). 1 – new nozzle; 2 – after $t_B = 6$ h; 3 – after $t_B = 9$ h; 4 – after $t_B = 20$ h

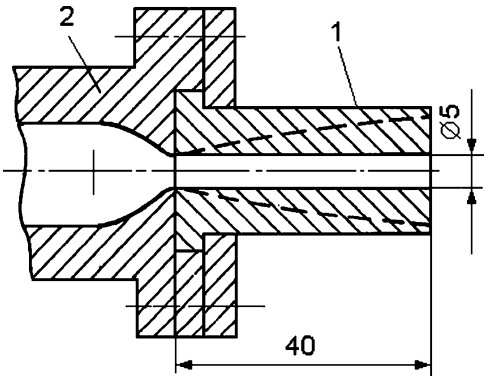

Fig. 4.40 Wear pattern in hardened steel blast cleaning nozzle with convergent entry section (Pashatskii et al., 1971). 1 – wear pattern after $t_B = 25$ min; 2 – nozzle body. Dimensions in mm

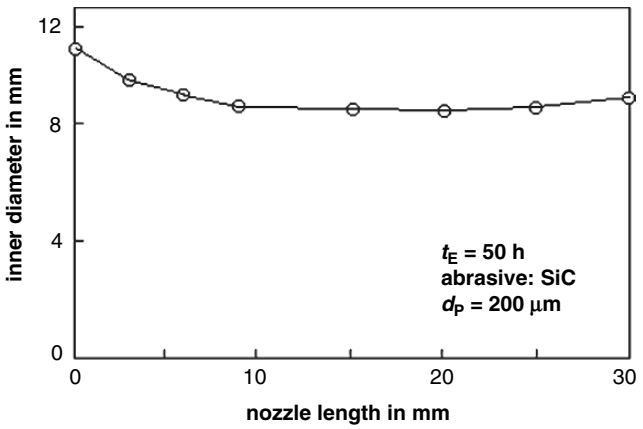

Fig. 4.41 Geometry of a ceramic blast cleaning nozzle after a performance time of 50 h (Deng, 2005b)

in Fig. 4.41. Originally, the nozzle had a cylindrical design, but it changed to a convergent–divergent shape over the time. This change in internal geometry may be one reason for the observation that used cylindrical nozzles sometimes perform better than new, unused cylindrical nozzles.

Worn nozzles should be replaced in time. It is not always easy to define a worn nozzle, but a general rule is: nozzles should be replaced if the (smallest) nozzle bore diameter is being increased between one and one-and-a-half millimetre. Results of quantitative wear measurements on a cylindrical blast cleaning nozzle are displayed in Fig. 4.42. It can be seen that both entry and exit bore diameters of the nozzle increased during the operation. After 9 h, the diameter of the exit bore was increased by about 1 mm; therefore, the value for the minimum diameter in the nozzle, which determines air mass flow rate and air velocity, had changed. The graphs also show a decrease in the wear rate (slopes of the curves) with an increase in operation time. The entry section, in particular, featured a very steep initial wear rate. These curves characterise nozzle wear as a non-stationary process. A quantitative comparison of the wear performance of different nozzles should, therefore, always be performed at operation times long enough to guarantee a stationary wear process. For the example plotted in Fig. 4.42, this critical operation time would be at about 8 h for the exit section.

Equation 3.9 illustrates that an increase in nozzle diameter is accompanied by a decrease in pressure in order to maintain the desired air flow rate. An example of how nozzle wear increased the volumetric air flow rate is shown in Fig. 4.43. The nozzle wear (in terms of diameter increase) shown in Fig. 4.43a followed a square-root relationship:

$$d_N(t_E) \propto t_E^{1/2} \tag{4.37}$$

Such a trend was also found on ceramic nozzles by Bothen (2001) and on steel nozzles by Pashatskii et al. (1971). However, the experimentally estimated increase

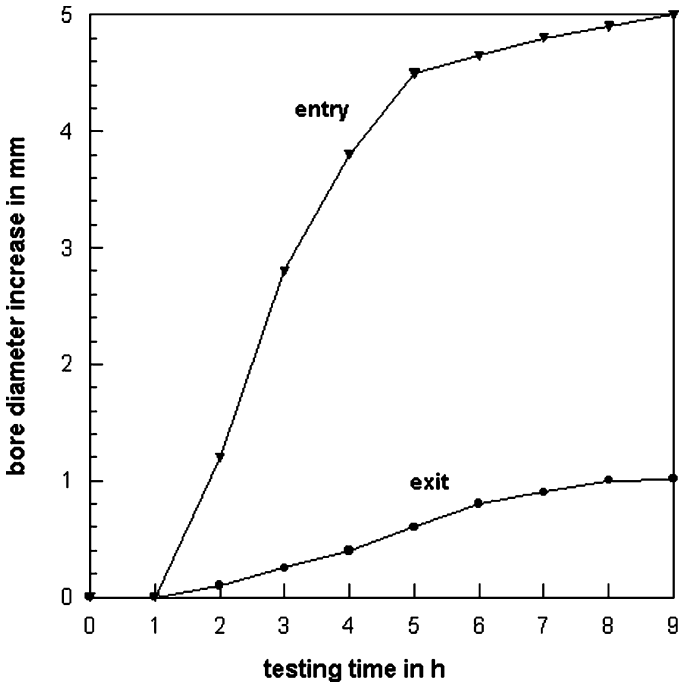

Fig. 4.42 Development of wear of blast cleaning nozzles (Deng et al., 2003a)

in volumetric air flow rate followed a linear relationship as shown in Fig. 4.43b. Because of $\dot{Q}_A \propto d_N^2$, this is not an unexpected result. If the compressor cannot deliver this demanded air flow rate, air pressure drops. According to (3.11), the relationship between nozzle diameter and nozzle air pressure is as follows:

$$d_N^2 \propto p^{-1} \tag{4.38}$$

A combination of $d_N = 12$ mm and $p = 1.0$ MPa delivers a volumetric air flow rate of $\dot{Q}_A = 13.5\,m^3$/min. If the nozzle diameter increases up to $d_N = 13$ mm, the reduced nozzle pressure is $p = 1.0\,\text{MPa}\cdot(12/13)^2 = 0.85\,\text{MPa}$. To compensate this pressure drop, the compressor must deliver a volumetric air flow rate of $\dot{Q}_A = 15.8\,m^3$/min (at $\vartheta = 20°C$). These calculations show that nozzle wear affects the working line of a nozzle. If the throat diameter of a nozzle is worn from originally $d_N = 10$ mm to 12 mm, the nozzle working line changes notably. This situation is illustrated in Fig. 4.3. The working point for the entire system changes from "II" to "III", and the system must be readjusted. Therefore, wear-resistant nozzles are a basic requirement for stable blast cleaning processes. If the compressor cannot deliver the desired additional volumetric air flow rate, the pressure at the nozzle drops, and the cleaning rate will be reduced. An example is provided in Fig. 4.37. It can be seen that the relative cleaning rate drops from originally 100% for $d_N = 8$ mm down to 64% for $d_N = 10$ mm. This particular example does not consider effects of abrasive hose lines ($l_H = 0$).

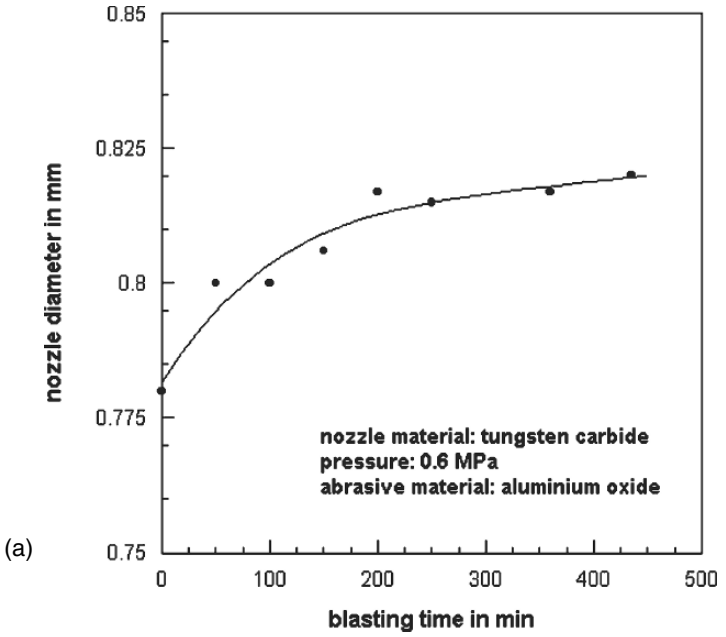

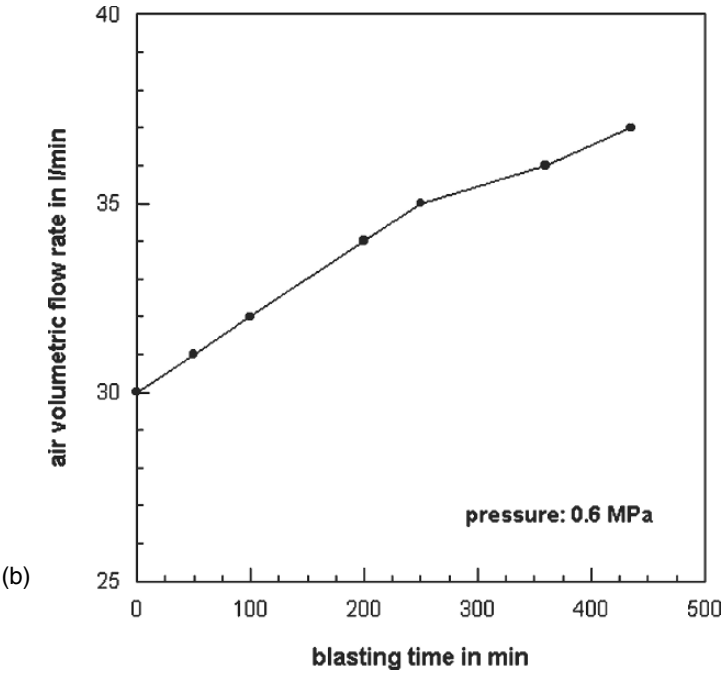

Fig. 4.43 Wear of a Laval nozzle (Bothen, 2000). (**a**) Increase in nozzle diameter; (**b**) Increase in air volume flow rate

4.6.2.2 Parameter Effects on Nozzle Wear

Nozzle wear depends on nozzle and abrasive parameters as well as on process parameters. Investigations into the effects of blast cleaning and material parameters on nozzle wear were performed by many authors.

It is known for more than 40 years (Adlassing and Jahn, 1961) that nozzles made from boron carbide featured the highest wear resistance, and that the use of aluminium oxide as an abrasive accelerated blast cleaning nozzle wear. More recent measurements verified these early results (Grearson et al., 1989). Results from site experience are listed in Table 4.11. The reason for the high wear resistance of boron carbide is its high hardness (see Table 4.12). A typical relationship between the erosion rate of tungsten carbide composites and hardness is as follows (Laugier, 1986):

$$E_R \propto H_N{}^{-3.5} \tag{4.39}$$

Figures 4.38, 4.44 and 4.45 illustrate the effects of nozzle material hardness. Results plotted in Fig. 4.44 show that an increase in nozzle material hardness notably improved the resistance of the nozzle to wear. It can be seen from Fig. 4.45, that the nozzle made from boron carbide experienced a much lower erosion rate compared with the nozzle made from aluminium oxide.

The influence of the abrasive type is illustrated in Table 4.11 and Fig. 4.45. From the materials listed in Table 4.11, corundum (aluminium oxide) abrasives caused the most severe erosion, which may again be due to the high hardness of this material. Figure 4.45 shows, however, that the intensity of nozzle wear is controlled by a combination of the hardness for nozzle material and abrasive material. Although the erosion increased for the alumina nozzle and for the boron carbide nozzle if the abrasive material hardness increased, the alumina nozzle was more sensitive to changes in abrasive material hardness. It will, therefore, basically be the hardness ratio between nozzle material and abrasive material, which determines wear resistance. This ratio is given as follows:

$$R_H = \frac{H_N}{H_P} \tag{4.40}$$

If the hardness ratio is high, wear rate is low and vice versa. These aspects are illustrated in Fig. 4.45, which shows that wear increased if abrasive material hardness

Table 4.11 Nozzle lifetime values (Kennametal, Inc., Charlotte)

Nozzle material	Approximate lifetime in h		
	Abrasive material		
	Steel shot/grit	Quartz sand	Aluminium oxide
Aluminium oxide	20–40	10–30	1–4
Tungsten carbide	500–800	300–400	20–40
Silicon carbide composite	500–800	300–400	50–100
Boron carbide	1,500–2,500	750–1,500	200–1,000

Table 4.12 Mechanical properties nozzle of materials (Deng et al., 2003a)

Nozzle material	Flexural strength in MPa	Hardness in GPa	Fracture toughness in MPa $m^{1/2}$
Boron carbide (B_4C)	350	32.5	2.5
Tungsten carbide (WC/8Co)	1,500	14.8	14.5
Alumina carbide (Al_2O_3/45C)	850	21.5	4.9

increased; but the absolute wear was always less for the boron carbide nozzle. The effect of the nozzle material hardness on nozzle wear is illustrated in Fig. 4.44. Erosion rate notably dropped if a nozzle material with a high hardness was utilised. The performance in terms of reduced wear could be almost doubled if a nozzle material with a hardness of $H_N = 23.8$ GPa [boron carbide composite, B_4C/50 wt.% (W, Ti) C] was replaced by a nozzle material with a hardness of $H_N = 32.5$ GPa (boron carbide, B_4C). Table 4.12 lists mechanical properties of some typical blast cleaning nozzle materials.

Nozzle geometry parameters, namely nozzle diameter and nozzle length, affect the wear performance as well (Adlassing, 1960; Kumar et al., 1983). Results of respective measurements are provided in Fig. 4.46. Nozzle mass loss, which expresses wear, increased if longer and wider nozzles were used. The relationship between bore diameter and nozzle mass loss was of a parabolic shape (Adlassing, 1960). An opposite trend was reported by Kumar et al. (1983) for the wear of very small steel nozzles ($d_N = 0.8$–1.6 mm). These authors found a decrease in wear for larger nozzle diameters. The effects of varying angles of the nozzle entry section on the wear

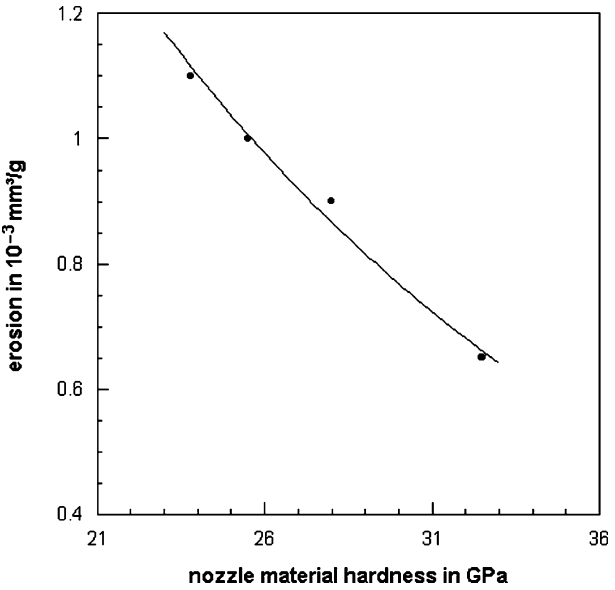

Fig. 4.44 Effect of nozzle material hardness on nozzle wear (Deng, 2005a)

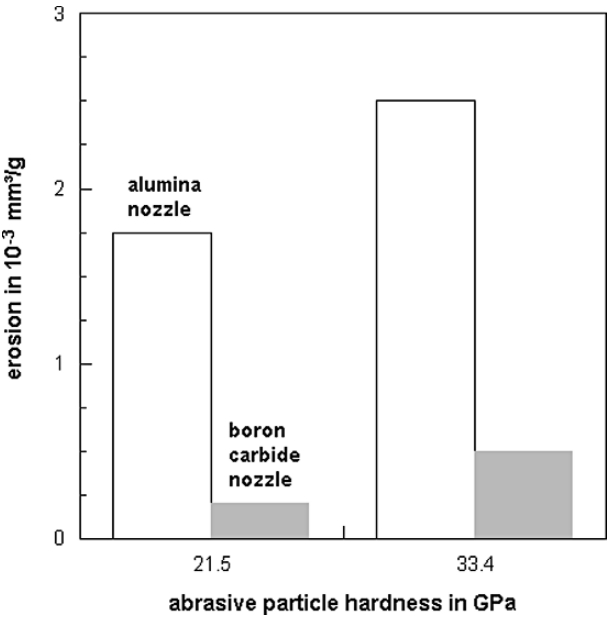

Fig. 4.45 Effect of abrasive material hardness on nozzle wear (Deng et al., 2003b)

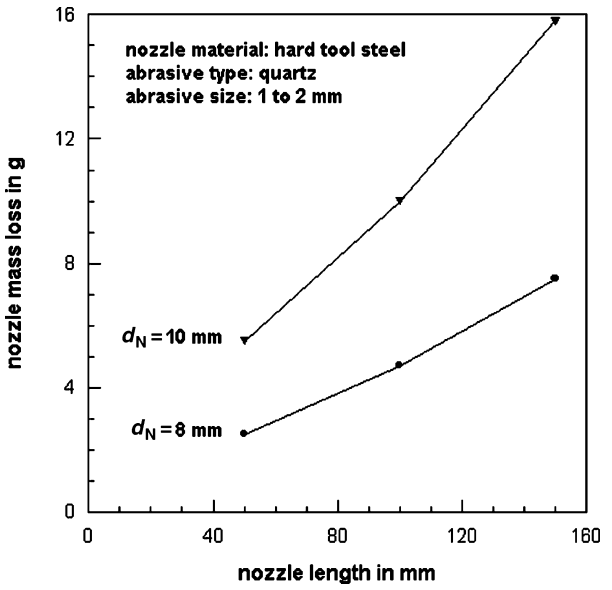

Fig. 4.46 Effects of nozzle length and nozzle diameter on nozzle wear (Adlassing, 1960)

of convergent-cylindrical steel nozzles was also investigated by Kumar et al. (1983), and they could prove that the wear increased for smaller entry angles. This result was contributed to an increase in the length of the convergent section of the nozzle.

Process parameters also affect nozzle wear. It was found by several authors that nozzle wear increased if air pressure rose (Adlassing, 1960; Pashatskii et al., 1971). Nozzle wear was also found to increase linearly if the abrasive particle concentration (Pashatskii et al., 1971) or the mass flow ratio abrasive/air (Kumar et al., 1983) was increased. Kumar et al. (1983) investigated the influence of the abrasive particle size on the wear of steel nozzles. They utilised small aluminium oxide particles ($d_P = 30$ and 38 µm), and they could show that the nozzle wear was more severe for the larger abrasive particles. However, a notable difference between the effects of the two different particle sizes was obvious at rather long exposure times only.

4.6.2.3 Wear Performance of Laminated Ceramic Nozzles

A new approach to increase nozzle lifetime is the utilisation of laminated ceramic nozzles (Deng et al., 2007). Due to the different thermal expansion coefficients and due to shrinkage of the individual layer materials, residual compressive stresses are generated in the laminated sections of the nozzle (entry and exit sections). These compressive stresses may partly balance tensile stresses which form during the erosion process in the nozzle. Figure 4.47 exhibits results of comparative wear tests.

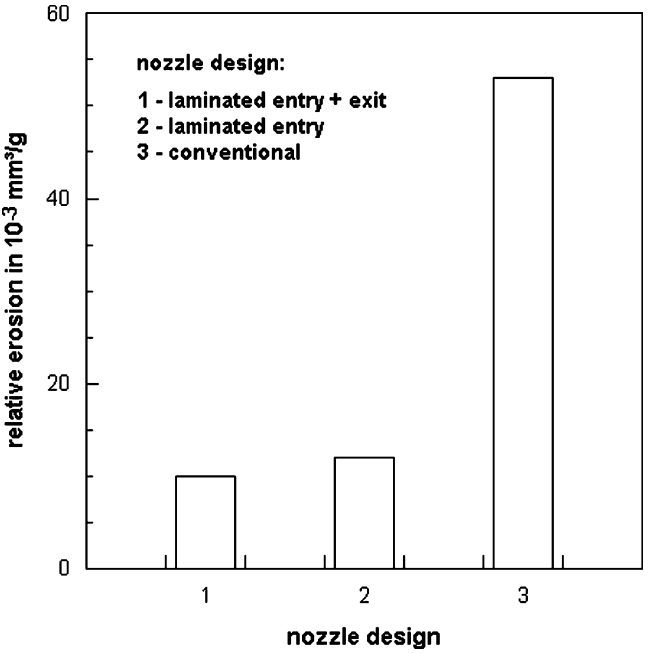

Fig. 4.47 Results of comparative wear measurements on conventional ceramic nozzles and laminated ceramic nozzles (Deng et al., 2007)

The standard nozzle exhibited the most severe wear. The nozzle with a laminated entry section performed better, but the best performance was delivered by the nozzle with laminated entry and exit section. Long-term (540 min) measurements of the entry bore diameter of different nozzles were also made. The entry bore diameter of a conventional nozzle increased up to $\Delta d_N = 7$ mm, whereas the entry bore diameter of a laminated nozzle increased up to $\Delta d_N = 1$ mm only (Deng et al., 2007).